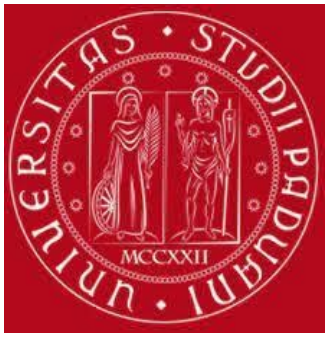

UNIVERSITA' DEGLI STUDI DI PADOVA

SCUOLA DI SCIENZE

Dipartimento di Geoscienze

Tesi di Laurea Magistrale

A comparative study using 3D measurement with ERT method and Ohm mapper instrument to assess soil water content and root system in a vineyard: a Case study in Montalcino, Siena, Italy

Relatore: Prof. Alberto Garfagnini

Correlatori: Prof. Fabio Mantovani

Laureando: Alireza Madani

ANNO ACCADEMICO 2023/2024

Abstract

Soil water availability deeply affects plant physiology. In viticulture it is considered a major contributor to the “terroir” effect. The assessment of soil water in field conditions is a difficult task, especially over large surfaces. New techniques are therefore required in order to better explore variations of soil water content in space and time with low disturbance and with great precision. This study focuses on a comparison between two geophysical surveys within an agronomic framework, involving the inversion of 3D ERT data from the galvanic contact resistivity (GCR) method and 3D data using ohm mapper from the capacitively-coupled resistivity (CCR). By minimizing misfit in model parameters, the inversion process enhances data-fitting in terms of resolution and accuracy of subsurface models within the inversion theory framework. Datasets were acquired in a red Sangiovese grape vineyard ("Tenuta il Poggione '' - Montalcino, Siena, Italy), covering a 225 m^2 area (15m×15m). Employing a 3D ERT configuration for maximum resolution perpendicular to the vineyard rows and 2D CCR sections along the rows, the study encompasses the vineyard’s root system. We compare the results from individual 3D ERT and CCR inversions, with the primary objective of assessing soil water content and root system more accurately. This study demonstrates the enhanced effectiveness and precision of both methods when applied to geoelectrical data in agro geophysical investigations.

Content Table

1. Acknowledgment

Almost three years of study at the University of Padova gave me a lot of new ideas and innovative knowledge. All these are achieved with great help from my supervisors, friends, colleagues, and my families.

Alberto Garfagnini is the first one who I would like to sincerely appreciate. He is the one who opened a door to a new life for me. I became familiar with him when I took advanced statistics for physics course and participated in classes, and helped me to learn many concepts related to coding. As main advisor he has intentionally trained me from many aspects, such as coding, data interpretation, presentation, etc. With a great effort he enlightened me in the data world, which lets me understand more about data analysis. When we were in the class together, he made the atmosphere enjoyable.

Fabio Mantovani as my co-supervisor is sincerely appreciated. Since I wanted to do my thesis in a company, Professor Garfagnini introduced me to him and he opened a new window for me to work at Geoexplorer company to improve my experience, and work on my thesis at the same time. He dedicated a lot of effort to help me in my research. He guided me intelligently and peacefully no matter what kind of problem I had. He transferred his experiences to me with great patience. We discussed my research results, manuscript, and writing thesis many times, even with limited time provided to him at Geoexplorer company.

Lastly, I extend my heartfelt gratitude to all my colleagues at Geoexplorer company, with particular appreciation for the company managers, Tommaso Colonna and Enrico Guastaldi, for affording me the opportunity to acquire valuable experience through my thesis work within the company. This experience has undoubtedly bolstered my resume.

2. Introduction

In viticulture and oenology, it is acknowledged that the natural environment has a major impact on the yield and vegetative growth of grapevines and therefore on the sensory attributes of the final product. This link between the characteristics of a wine and its origin is called the “terroir” effect. This relationship is not mediated through the effect of particular soil minerals or flavor compounds, although the popular wine press often erroneously describes it thus. The terroir effect must be sought in interactions at the ecosystem level. One of the Major factors in the terroir effect are the supplies of water. Water is a major driver of vine physiology at the whole-plant level.

This research focuses on soil and vine water relationships. Soil is not a homogeneous medium, and is therefore not explored by roots in a homogeneous way. Hence, during drought, soil cannot dehydrate in a homogeneous way. It is surprising that such evidence is often neglected, and that available soil water capacity is generally considered a soil characteristic, independent of the plant. The highly variable spatial-temporal distribution of wet and dry zones in soils has profound physiological implications for plants. Indeed, while chemical and hydraulic root signals are produced in moderately dry soil regions, the part of roots in wet soil regions ensures the supply of water and therefore transpiration and photosynthetic activity.

Partial root zone drying (PRD) is an irrigation concept based on this knowledge. It maintains reasonably high yields because vines pick up water from the wet soil zones, while quality is high because roots produce Abscisic Acid (ABA) in the dry zones of the soil profile. In natural conditions, such spatial soil water heterogeneity can also be found. The magnitude of such variations in soil moisture and their impact on vine physiology has rarely been studied. Soil moisture spatial variations might play a key role in the terroir effect. In a recent review, remarked that soil water (SW) monitoring is a challenging task because root distribution is generally

unknown and it is therefore difficult to understand how much water is effectively absorbed in each soil layer.

The reason why such spatial variations in soil water availability have rarely been considered is that, at present, soil water measurements are generally obtained with in-soil devices such as time domain reflectometers (TDR), which can be difficult to use in field conditions. Furthermore, these devices only measure a very small volume of the soil, and even when the number of probes is increased, no information is generally obtained about the lateral variation of SW and only a vertical soil moisture profile can be established. In addition, the number of such devices cannot be increased indefinitely without major perturbations of the system and incurring prohibitive costs.

Geophysical imaging techniques, which are rapid, cost-effective and cause only low perturbation of the soil, have recently been proposed as a good proxy for the spatialization of soil water measurements. This research concentrates on soil water content and root system in a specific vineyard, using 3D ERT and ohm mapper methods to spatially measure soil water and its availability to plants. In the first step, we describe the environment and environmental factors that can affect the quality of grapes in the vineyard. Then, after explaining the geophysical method of ERT and the ohm mapper instrument, we will discuss how to collect data using these methods. In the last step, after obtaining the three-dimensional model resulting from the mentioned methods, we will compare them in order to deeply understand the soil water content and the root system and everything that happens in the subsurface.

3. Site

3.1. Montalcino Town History

Montalcino is a small town located in the Tuscany region of Italy, known primarily for its wine production. Its historical development is deeply intertwined with the broader history of Tuscany and Italy. The area around Montalcino has a history dating back to the Etruscan and Roman periods. Archaeological evidence suggests that it was inhabited during these times, with Roman roads passing through the region. The town was known as "Mons Lucinus" during Roman times. Montalcino's medieval history began in the 9th century. It was initially a small settlement, but over time, it grew and developed, particularly as a fortified hilltop town. Like many towns in medieval Italy, Montalcino experienced a feudal system with various noble families vying for control.

The Aldobrandeschi family, who had control of the town during the 11th and 12th centuries, played a significant role in its development. In the 13th century, Montalcino came under the influence and control of the Republic of Siena, a powerful city-state in Tuscany. This marked a significant period of change and growth for Montalcino, as it became a crucial part of the Sienese defense system. Montalcino was a loyal and strategic outpost for the Republic of Siena, contributing to the city-state's military and economic activities **(Figure 3.1)**. This period saw the construction of the town's impressive fortifications, some of which still stand today. In the mid-16th century, the Republic of Siena fell to the Republic of Florence, marking the end of Sienese rule over Montalcino. The town then became part of the Grand Duchy of Tuscany under the Medici family.

The first train arrived in one of Montalcino’s hamlets, Torrenieri, in mid-19th century, connecting the isolated town to the rest of Italy and civilization. It was at about this time that a few of Montalcino’s wealthy gentlemen farmers, most of whom already made a well-known sweet white wine called Moscadello, began experiencing with red wine, eventually leading to the creation of Brunello. [1]

Today, Montalcino is renowned for its wine and is a popular tourist destination, drawing wine enthusiasts and history buffs alike. The town is known for its well-preserved medieval architecture, including the impressive Montalcino Fortress, which offers stunning views of the surrounding countryside.

Montalcino's rich history, picturesque setting, and exceptional wine production have made it a significant cultural and economic center in Tuscany. It continues to be a symbol of Italian winemaking excellence and a must-visit destination for travelers exploring the region **(Figure 3.2)**.

Figure 3.1. Montalcino's imposing 14th century fortress protected the republic of Siena from Florence in mid-16th century

Figure 3.2 Montalcino aerial view

3.2. Montalcino Wine History

Montalcino's wine economy has navigated through periods of challenge and prosperity, with significant milestones in the early 19th century shaping its trajectory. Traditionally, the region's financial backbone was its land, primarily controlled by a single social class. This class relied on traditional, sharecropping-based practices, constituting around 95% of agrarian production. However, a turning point emerged in the mid-19th century with Clemente Santi's groundbreaking efforts. Amid socio-economic stagnation, Santi initiated scientific studies, particularly focusing on grape and olive cultivation, introducing advanced agrarian techniques.

The 1880s witnessed a new generation of Montalcino winegrowers led by Ferruccio Biondi Santi, Clemente Santi's grandson. Leveraging his grandfather's expertise, Ferruccio dedicated himself to the "Greppo" vineyards. Employing a meticulous approach, he selected and replanted Sangiovese grapes, rejuvenating his vineyards through grafting and careful cultivation. In 1888, he produced the inaugural Brunello, a historic vintage with two preserved bottles still held in the Biondi Santi family's cellar.

Ferruccio's commitment extended to deliberately limiting yields to ensure superior grapes. He retained only the best bunches, resulting in a Brunello with high tannin levels and elevated acidity. He championed slow aging in Slavonian oak barrels, a practice integral to Montalcino's wine production today. The outbreak of World War I prompted some winegrowers to abandon vineyards, leading to a decline in Montalcino's wine interest. Ferruccio Biondi Santi passed away in 1917, and the early 20th century saw a diminished enthusiasm for Montalcino wine due to restrictive agricultural policies in Italy.

Tancredi Biondi Santi, Ferruccio's son, persisted in wine production, founding a wine cooperative in 1926. His significant contribution was "ricolmatura," enhancing wine quality in old bottles by replenishing losses. However, it wasn't until the 1950s and 1960s that these experiences evolved into a more developed viticultural landscape. World War II inflicted damage on the Tuscan countryside, impeding improvements to Montalcino's vineyards. In the post-war years, the population declined significantly, indicating economic challenges.

The 1960s brought relief with the enactment of a framework law protecting wines, leading to Brunello receiving DOC status in 1966. This marked a crucial recognition of the wine's superior characteristics. However, it became apparent that DOC designation alone couldn't safeguard Montalcino wine quality, leading to the introduction of the DOCG designation in 1980. Montalcino welcomed foreign investments, with Villa Banfi playing a pivotal role. The American company's influence, starting in 1977, opened doors to the international market, making Montalcino wines globally recognized.

Villa Banfi's significant investments positioned it as the largest wine estate in Montalcino, contributing to the region's international visibility. Subsequently, other foreign companies, from Switzerland, Germany, England, and more recently, Argentina, Panama, and Brazil, followed suit. These investments have not only contributed to the economic vitality of Montalcino but have also fostered a global appreciation for its exceptional wines. [2]

In this chapter, the main goal was a better understanding of historical development of Montalcino's wine from 19th century that can be helpful in order to know Montalcino's wine rich history, moreover significance of that specific area, in terms of history, wine production, wine quality, and popularity, convinced me to work on Montalcino region as a thesis.

3.3. Environmental Factors

Viticultural zoning, a complex and crucial practice in the world of winemaking, revolves around the meticulous division of geographical regions into distinct zones, with the overarching goal of maximizing the uniformity of environmental influences on grape quality. This process hinges on the careful consideration of four primary environmental factors: climate, physiography, geology and soil conditions. To fully grasp the essence of viticultural zoning, we must delve into the concept of environmental heterogeneity, a cornerstone in understanding the diversity of "terroir" and its profound impact on wine quality. Environmental heterogeneity is inherently tied to the spatial and temporal variations of environmental factors, making it a pivotal factor in the art and science of winemaking. [3]

1. **Physiography:** Physiography, the first critical component of viticultural zoning, encompasses variables like altitude, slope, aspect, and topographic position. Each of these factors exerts a unique influence on the growth of grapevines and the ultimate quality of the grapes. Altitude, for instance, is often linked to temperature. Slope, on the other hand, affects erosion, soil depth, and the mechanical aspects of vineyard management, introducing complexities that winegrowers must navigate. Aspect, another aspect of physiography, impacts radiation balance and air temperature, further shaping the terroir of a given region.

   From a topographical point of view, land surface exerts a profound impact on agriculture, as it has the capacity to bring about localized modifications in climate and weather patterns. In many cases, it stands as the predominant factor that dictates the suitability of a particular part of land for various forms of farming. The presence of mountains and hills can wield significant influence over rainfall distribution. It is not uncommon to witness a stark contrast between a dry, irrigated valley on one side of a mountain range and a wetter, rainfed valley on the opposite side. These variations can create distinctive microclimates within relatively small geographical areas. [4]
2. **Climate:** Climate, the second of the four core factors, encompasses elements like temperature, water, and incoming solar radiation, which play a fundamental role in the growth and development of grapevines. The variation in climate significantly contributes to the diversity of wine produced in different regions, as it shapes the characteristics of the grapes. Temperature is a critical factor in determining the types of crops that can be grown and their growth cycles. Different crops have specific temperature requirements for germination, growth, and maturation. In general, the higher the temperature, the faster these processes occur. The size, quality and shape of storage organs are greatly affected by soil temperature.

   In terms of water factor, vine water status depends on soil texture, percentage of stones, rooting depth, rainfall, evapotranspiration, and leaf area. [5] Rainfall patterns, which are influenced by geography and climate, determine the availability of water for vine. Regions with consistent rainfall can support a wide variety of vine, while arid regions require

irrigation to sustain agriculture. Excessive rainfall can also lead to problems like waterlogging.

Rooting depth is a key component in a vine's ability to access water. Deeper root systems in grapevines allow for a more extensive network for water uptake. Grapevines with shallow root systems are more susceptible to water deficits, which can be a significant problem during periods of drought or water scarcity. Different grapevine species may exhibit variation in the horizontal and vertical depth distribution of their root systems. This variation may have both genetic and environmental components. [6]

Soil texture is a fundamental determinant of a vine's water status. The composition of the soil, whether it is sandy, loamy, or clay-rich, affects its water-holding capacity and drainage. Vineyards with sandy soils tend to drain water more quickly, potentially leading to water stress, while clay-rich soils may retain moisture for extended periods, reducing the risk of water deficit. [7]

Also, Soil texture may influence rooting patterns in the sense that fine textured soils would have higher water-holding capacities, lower resistances to water extraction, and shallower infiltration rates than coarse-textured soils. So, it might be predicted that root systems in fine textured soils would be smaller and shallower and, conversely, those in coarse-textured soils deeper. the vine root depth range is from 0.5 to 2.5m, but more than half of the root system is concentrated at depths between 0.25 and 0.5 m. [8]

evapotranspiration is a measure of the water loss from the soil through evaporation and transpiration from healthy, well-watered plants. When ET0 exceeds the available water supply, it can lead to water deficit stress in grapevines. This condition impairs photosynthesis, and reduces shoot growth. [9]

Leaf area plays a critical role in the production of carbohydrates (photosynthate) through photosynthesis and water status. The amount of photosynthate produced by a vine is a key determinant of how much fruit it can ripen. More leaf area generally means more photosynthate supply, which can support the growth and development of the grape crop. A certain amount of leaf area is necessary to adequately ripen a gram of fruit, typically ranging from 7 to 12 cm^2 of leaf area per gram of fruit. [10] A larger leaf area can lead to

increased transpiration, potentially exacerbating water stress during periods of insufficient water availability.

Solar radiation plays a central role in generating atmospheric circulation. It is the energy source that drives the movement of air masses, which, in turn, affects weather patterns and climate in a given region. Solar radiation is a primary determinant of temperature in an area. The amount of solar radiation received influences the local climate, including temperature variations. [11]

3. **Soil**: The third and key element in viticultural zoning is the soil, which varies in physical and chemical parameters across different regions, profoundly affecting the growth of grapevines. Soil chemistry is strongly influenced by the underlying rock, except in the case of alluvial soils. Different types of rocks can contribute various minerals and elements to the soil, affecting its composition. This geological factor plays a significant role in the characteristics of the soil in a vineyard. chalk most consistently provides the ideal porosity and permeability for viticulture. However, moderately cemented, fractured limestones other than chalk, sandstone and conglomerate will also frequently fulfil the criteria for the ideal water balance, as can deeply weathered and fractured schist or granite. Where the slope bedrock is impervious like shale, drainage through the rock is extremely slow and most water will move down slope as surface runoff, taking soil with it. Grapevines, like most plants, require essential nutrients, including nitrogen (N), phosphorus (P), potassium (K), magnesium (Mg), and iron (Fe), for their growth and development. Different nutrients are needed for specific purposes within the vine, such as leaf growth (N, Mg, Fe) and flower and fruit production (K, P). [12]

   The surface characteristics of the topsoil also play a significant role in the thermal behavior of the vineyard. For instance, stony soils, especially if they are pale-colored, have the ability to reflect heat. This characteristic can have a substantial impact on the climate of the vineyard.

4. **Geology:** The last element in viticultural zoning is the geological setting. Vineyard geology is the rock type and sedimentary strata, including the areas of bedrock where wine is grown. With the exception of vineyards established on alluvial deposits, such as those found on valley floors or alluvial fans, the majority of vineyard soils are intricately linked to the bedrock beneath them, or the bedrock in the immediate upslope area. The character of this underlying bedrock, as well as the extent to which it has weathered, wields a substantial influence over the physical properties of the soil. These properties, in turn, have a significant impact on the growth of vine roots. In fact, it is the substrate properties that often exert a greater influence on root growth than the genotype of the rootstock itself. Additionally, these properties play a crucial role in the management of vineyards. [13]

   Also, Geology can influence a vineyard's drainage characteristics. Soil with a high percentage of clay, silt, or organic matter may retain water, while sandy soils drain more freely. The balance between drainage and water retention is crucial for vine health and grape quality. The structure of the underlying rock can determine how deep vine roots can penetrate. Rocky soils may limit root growth, potentially affecting the vines' access to water and nutrients.

So, the concept of terroir is at the heart of the interaction between geology and wine. Terroir refers to the unique combination of factors, including geology, climate, and human influence, that shape the character of a wine. Each vineyard has its own terroir, which imparts specific flavors, aromas, and textures to the grapes and, ultimately, the wine.

In the next step, we'll start with an analysis and also a description of the territory of Montalcino in order to have a better understanding of all environmental factors that can influence vine growth.

3.3.1. Regional Setting

The study area is located in the territory of the Montalcino town (43°03'18"N 11°29'20"E), the southern part of the province of Siena **(Figure 3.3)**. Its western boundary is marked by the Ombrone River, a crucial water feature in this part of Tuscany, while its southern limit is defined by the Orcia River, a significant eastern tributary of the Ombrone **(Figure 3.4)**.

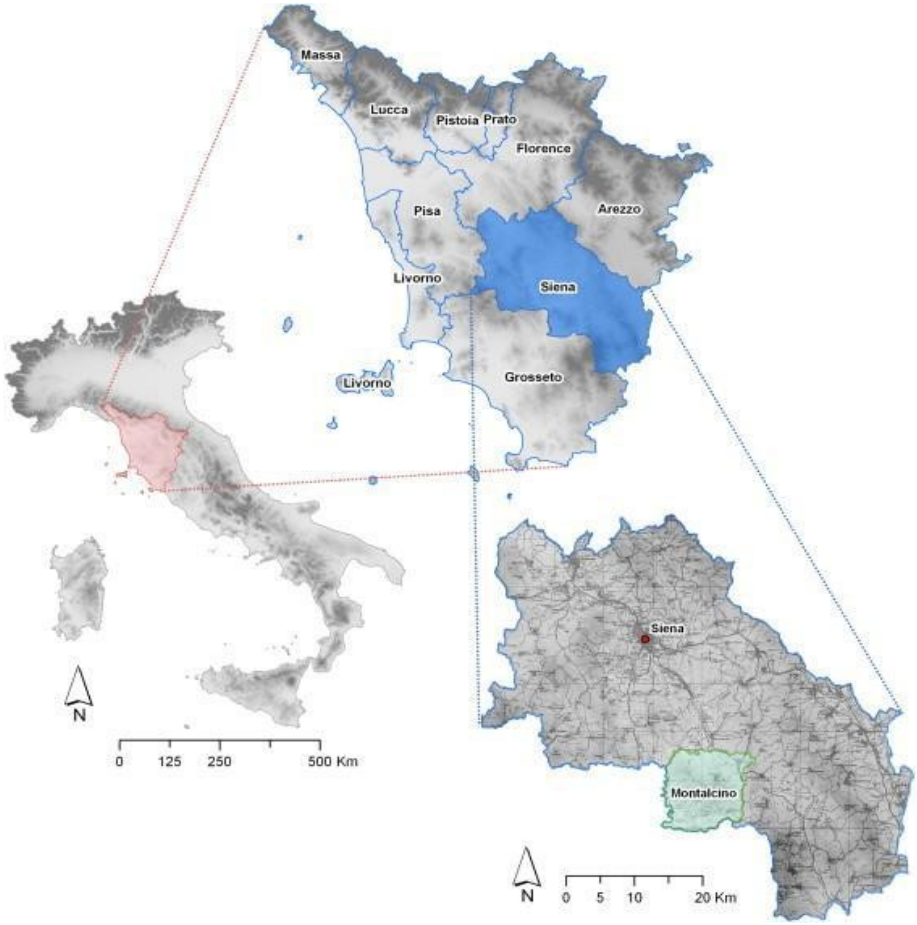

Figure 3.3. Montalcino, Province of Siena, Italy

This area displays a varied landscape between hilly terrains formed during the Mio-Pliocene and Pliocene periods and more elevated formations, predominantly originating from the pre-Neogene era with features of Tuscan or Ligurian geology. Within this context, Montalcino serves as a unifying presence, extending its influence over both these environments.

The territory is traversed from its northwestern edge, where it meets the municipality of Murlo, to its southeastern boundary, by the Montalcino Ridge **(Figure 3.4)**. This ridge acts as a natural divider, separating the Siena Basin from the lower Vald'Orcia. The geological formations here belong to the Ligurian units [14]. The Montalcino Ridge exhibits mountain-like characteristics, with altitudes ranging from 500 to 600 meters above sea level **(Figure 3.5)**.

Figure 3.4 Geographical position, Montalcino, Province of Siena

In the southern part of the municipality, you'll find terrain reminiscent of the medium-lower Val d'Orcia basin. The areas near Val d'Orcia, Montalcinesetra, La Velona, and Sant'Angelo in Colle (the study area is located in Sant'Angelo in Colle) are characterized with attitudes ranging from 200 to 300 meters above sea level **(Figure 3.4)**.

To the west, from Sant'Angelo in Colle up to Camigliano, the landscape is marked by plateaus such as Campo Giovanni, Argiano, and Poggio alle Mura **(Figure 3.5)**. These areas are largely comprised by Pliocene clays, resulting in the characteristic progression of vegetation-scarce hills, often shaped by erosive forces.

Figure 3.5 view of the municipality of Montalcino from Sant' Angelo in Colle

Another geological variation in Montalcino includes plains and terraces located near the main watercourses. Along the northern course of the Ombrone, between Montalcino and Buonconvento, the presence of clay has given rise to extensive alluvial plains and terraces.

To the west, where the Ombrone River meets the Murlo territory, you'll find ophiolitic formations of the Murlo-Montacino ridge, leading to a sudden narrowing of the valley and a shift in vegetation towards woody cover **(Figure 3.4)**. The alluvial plain becomes more expansive only toward the end, near the confluence with the Orcia River.

In the southeastern part of the municipality, aligned with the slopes of Mount Amiata, the Orcia River traverses the Montalcino ridge once more. Along the border area with the municipality of Cartiglione d'Orcia, the Orcia Valley narrows, with sloping terrain densely covered in woodland vegetation. Midway along this course, the Orcia River meets the Asso River **(Figure 3.4)**. In the Montalcino section, the Vald'Asso extends in a north-south direction. In the southern segment,

you'll find Flyscharenaci, argillitic Fleysch, and polygenic conglomerates, resulting in a narrow valley. The northern stretch is marked by clay deposits, forming an extensive alluvial plain.

The central-eastern and southern regions include the surroundings of Montalcino, the area delimited by the road leading from Montalcino to Sant'Antimo and Sant'Angelo in Colle, as well as the lower Val d'Orcia **(Figure 3.4)**. These areas, once characterized by diverse crops like woods, arable land, olive groves, and orchards, are now primarily dedicated to Rosso and Brunello di Montalcino vineyards. This transformation has significantly altered the landscape, particularly in the Orcia vicinity and around Montalcino, leading to a shift towards monoculture.

3.3.2. Geological Setting

The Montalcino territory from a pedological point of view, are classified into four distinct types distributed across various parts of the territory [15]:

- Clays, primarily argillitic lithofacies of Pliocene origin with clayey galestro soils alternating with masses of alberese, predominate in the northeastern region of the municipality. They stretch from Torrenieri to the south, along the slopes of Montalcino, and eastward to the Asso River, particularly in the Sorgenti Alcaline area. These marine clays extend westward to the border of the Murlo municipality **(Figure 3.6)**. Going up we find marl where the clay gradually gives way to limestone systems. Going further up the terrain becomes richer in sandstone.

- The lithofacies, which are predominantly clay, characterize the north western expanse of the territory, encompassing a large area extending from the alluvial plain of the Ombrone in the west to the hills of Poggio Mulino a Vento and Poggio Pinzuto in the east. They also reach southward to the localities of Poggio ai Sassi and Costone, near Tavernelle **(Figure 3.6)**. This side of Montalcino is the least exploited for viticulture and where there are still

large extensions of woods. Also, in this area we find the typical Montalcino soil with limestone from marl and schist alternating with areas of clay or sandstone.

- Polygenic conglomerates with intercalations of marine clay and pebbles, alternating with outcrops of predominantly clayey lithofacies, define the south western sector of the municipality. These formations are found from Camigliano to the Ombrone confluence in the west and extend eastward to the Pentolaio area **(Figure 3.6)**. To the south, they reach the La Sesta farm, situated between S. Angelo in Colle and Castelnuovo dell'Abate. Also, we can find marly limestone and alluvial deposit soils on which large extension of vineyards have found space. This side of Montalcino is the least exploited for viticulture.

- The south eastern part of the Montalcino district is the most diverse, featuring alternating predominantly sandstones intermixed with marine clays and pebbles. Additionally, predominantly clayey lithofacies and isolated alluvial deposits are present in this varied environment. This diversity spans from the south of Montalcino to the course of the Orcia River, including the area of Castelnuovo dell'Abate **(Figure 3.6)**. Also, in the direction of Monte Amiata the soils are composed of sandstone and marl rocks with the presence of tuff of volcanic origin.

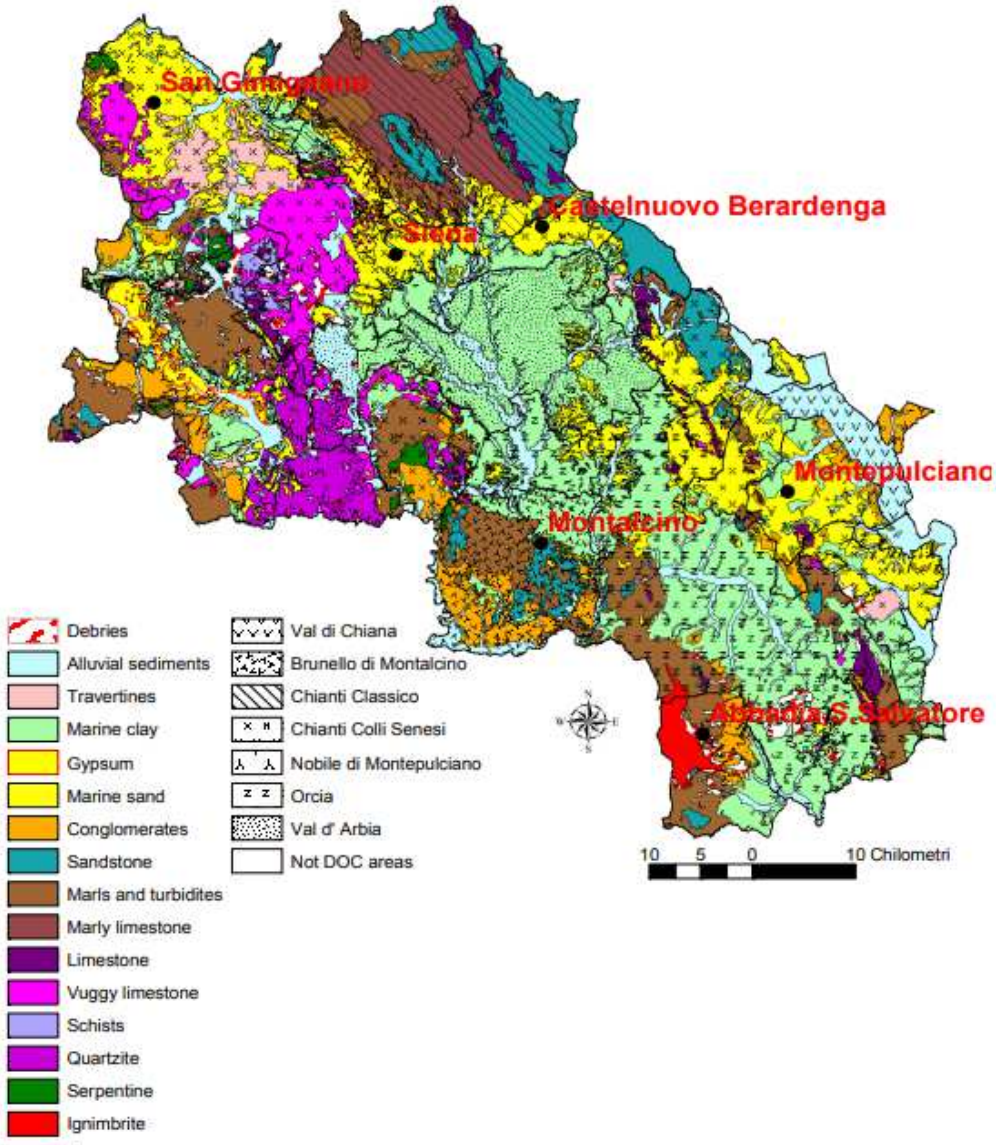

Figure 3.6 Classified Geological Mapping, Montalcino, province of Siena

3.3.3. Climate

From a climactic point of view, the province of Siena experiences a significant range in its average annual rainfall, spanning from 600 to 1300 millimeters **(Figure 3.7)**. This diversity in rainfall is

notably influenced by the region's topography. To elaborate, Mount Amiata in the southwest and the "Dorsale medio Toscana" along the western edge of the province, in addition to the famous "Chianti hills' ' to the east, serve as catchments for a substantial amount of rain. In contrast, the vast valleys nestled between these geographical features, namely the Elsa River and Orcia river valleys, exhibit minimal rainfall levels.

The average annual air temperature varies significantly, spanning from 10.2°C on Mount Amiata and to 14.8°C in the lower sections of the Elsa and Orcia river basins. However, the south facing slope of Montalcino presents the peculiarity of having a warm climate. The mean annual soil temperature at a depth of 0.5 meters reveals a different pattern compared to air temperature. This distinction is primarily due to the predominance of coarse-textured soils in the eastern part of the province and finer soils in the western regions. GIS becomes evident that the hilly belt ranging from 200 to 400 meters is the preferred choice for most farmers. This specific area receives an average annual rainfall of approximately 700-800 millimeters, maintains a long-term mean annual air temperature of around 13.5°C, and exhibits a soil temperature hovering around 14.8°C [16] **(Figure 3.8 and Figure 3.9)**.

In the Montalcino region, the climate is distinctly Mediterranean in nature, featuring a general aridity with characteristics of a continental climate due to its intermediary location between the sea and the Central Apennines. This geographical positioning results in considerable temperature fluctuations spanning from winter to summer. The distribution of rainfall primarily concentrates in the spring and late autumn months, contributing to an annual average rainfall of around 700 millimeters, in particular case, average annual rainfall in our case study (poggine vineyard) varies, and also is high, spanning from 750 to 850 millimeters **(Figure 3.7)**. During winter, particularly at altitudes surpassing 400 meters, the occurrence of snowfall becomes a possibility. Remarkably, the mid-hill regions experience infrequent encounters with fog and late frosts, a phenomenon partly owed to the significant air circulation in the area. This steady airflow fosters optimal conditions for the vitality of plants and fruits while preventing the stagnation of moisture [17]. Also, Montalcino vineyards are noteworthy for their high average of soil temperature and air

temperature, have been measured around 15° **(Figure 3.8 and Figure 3.9)**, but about poggine vineyard, soil temperature and air temperature average can be exceeded up to 17°. But research has shown that sometimes the air temperature and also soil temperature are higher than common temperature in Montalcino's vineyards, specially between spring and summer and in particular case, Poggione vineyrad **(Figure 3.10)**. Air temperature can reach up to 30°C and soil temperature in the same period varies, spanning from 23°C and 28°C [18].

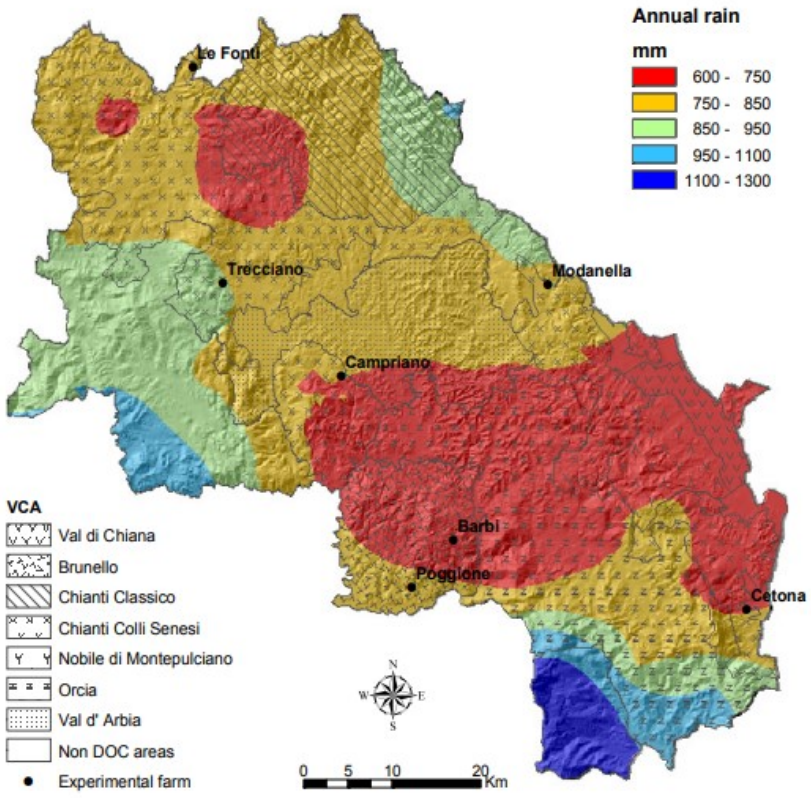

Figure 3.7 mean annual rainfall, province of Siena

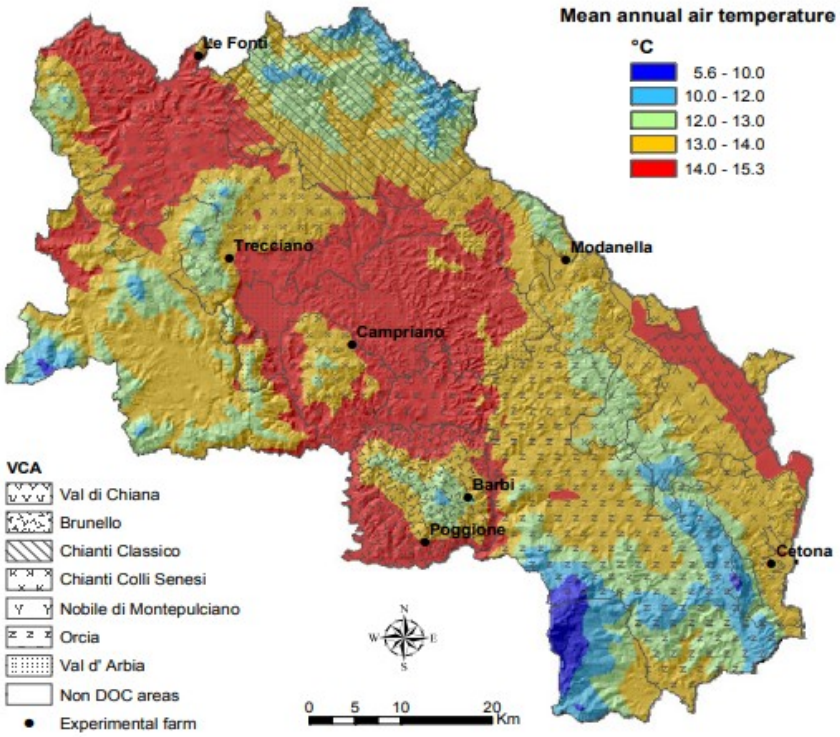

Figure 3.8 mean annual Air Temperature, province of Siena

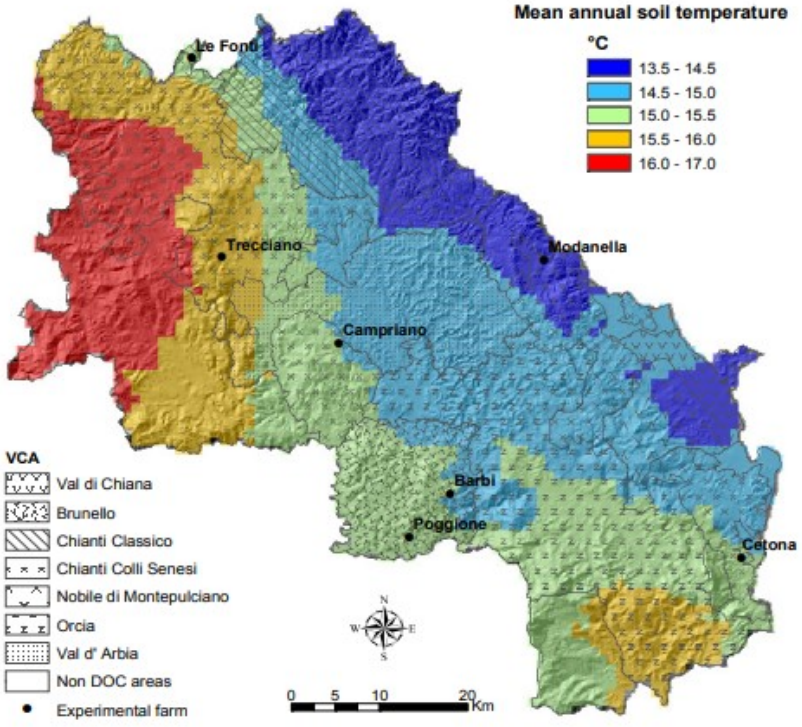

Figure 3.9 mean annual Soil Temperature, province of Siena

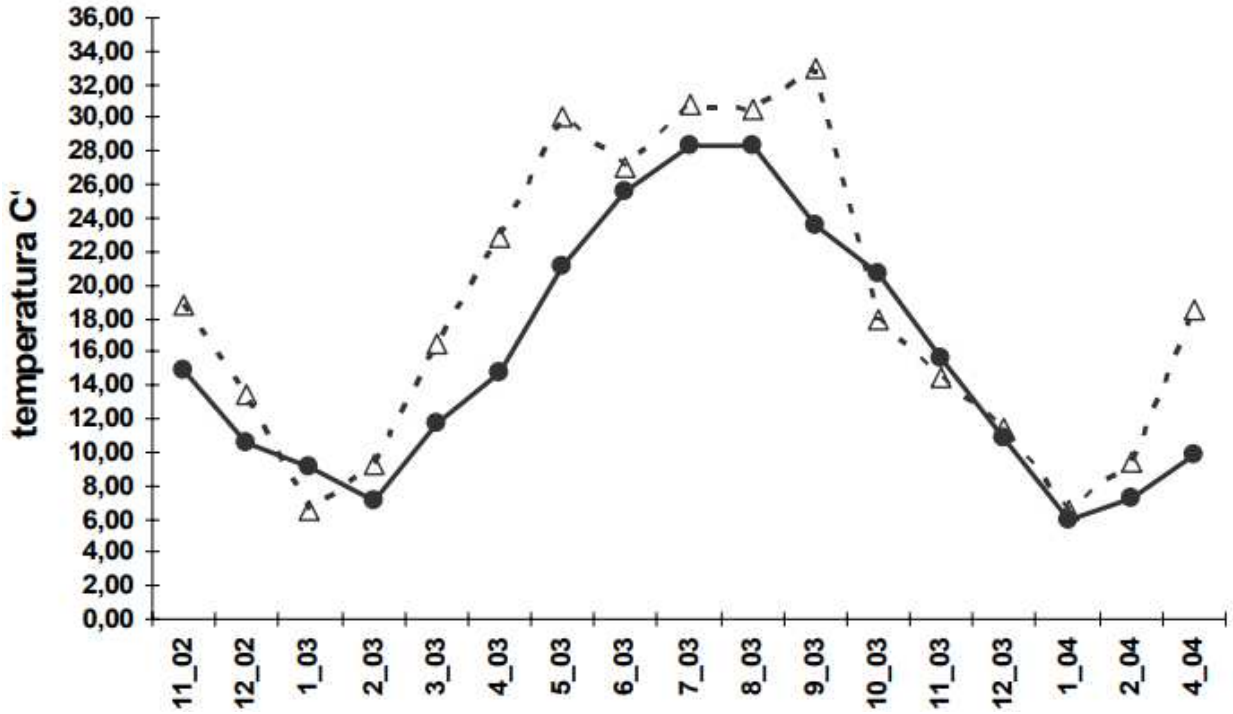

Figure 3.10. Air temperature and soil temperature, Poggione vineyard, Sant' Angelo in Colle, Montalcino

3.3.4. Soil Characterization

It is known that the aptitude evaluation of the territory for specific uses requires knowledge of the characteristics of the territory. This is achieved not only through surveys on the forms of the landscape, and climate, but also through field surveys and basic studies which allow the organization of a complete and reliable database on which to set the subsequent processing. On the basis of the analysis, it was therefore possible to carry out the examination of the stationary characteristics and the physical, hydrological and chemical parameters of the vineyard's soils of the provincial territory of Montalcino. The analysis was conducted at two different levels of detail:

- Analysis of soil characteristics in vineyards which are located in the Montalcino area.
- Analysis of soil characteristics in a specific vineyard which is located in Sant' Angelo in Colle (Poggione vineyard) **(Figure 3.11)**.

Figure 3.11. Poggione vineyard, Sant' Angelo in Colle, Montalcino

According to the available information of the characteristics of the soil in the Montalcino's vineyards area [19], highlights the typically hilly character of the Montalcino territory. The average altitude of the stations is 276 m above sea level, with 80% of the vineyard soils between 100 and 500 m altitude which is the best area for farming **(Table 3.1)**. 50% of these soils lie on slopes with a slope >7.6%, but the total soils occupy surfaces with a slope between 0 and 24% **(Table 3.1)**. 80% of the soils on sloping surfaces have an exposure between 45 and 338 degrees **(Table 3.1)**. Relative to the useful depth, the depth affected by the presence of roots, the vineyard soils of territory have an average value of almost 1 m **(Table 3.2)**; 80% of the soils have a useful depth between 60 and 130 cm, therefore classifiable from " moderately high " to "high. The soils are characterized by an average surface stoniness (percentage of ground coverage by rocky materials with diameter <500 mm) of 7.8% **(Table 3.2)**. These are therefore soils that can be classified as frequently stony (3-15%), which generally do not present strong limitations to mechanical processing.

The skeleton, the quantity of lithoidal fragments with a diameter >2 mm, represents on average 22.4%, a quantity that places the soils of the provincial territory in the frequent skeleton class (15-35%) **(Table 3.2)**.

From a hydrological point of view, it is noted that the internal drainage class that occurs most frequently (modal value) is class 3 (well-drained soils); at the same time, however, it is observed that 50% of the soil's present problems with water transmission along the profile, finding their place in classes with a score greater than 4 (median value), from "moderately well drained" to "very poorly drained". These are therefore soils that remain moist on the surface for rather long periods and which often require hydraulic regulation interventions. In the absence of such interventions agricultural activity is difficult and the soil can negatively affect normal cultivation practices and operations and the growth of plants **(Table 3.2)**.

External drainage, a parameter that evaluates the loss of water through flow on the soil surface, is in 50% of cases (median value 4) from "medium" (class 4) to "very high" (class 6). When assigning the external drainage class, the slope of the station is also taken into consideration; the nature of the soil therefore contributes to determining a general vulnerability of the territory to water erosion phenomena **(Table 3.2)**. The soils have, on average, moderate water availability (106 mm); more than half of the soils have "moderate" to "very high" volumes of water available for plants (AWC > 100 mm), and also, the bulk density of soils is generally 1.36 g cm-3**(Table 3.2)**.

The swelling and contraction potential of these soils, assessed by determining the coefficient of linear extensibility (COLE), is moderate (average value 4.37%). 90% of the samples analyzed have COLE values lower than 6%; we are therefore not in the presence of soils capable of limiting the development of plants due to strong water stagnation phenomena or damage to the root systems. Having a high content of 33.5%Clay, 35.4%Sand, and %31.1Limestone is a determinant of a quality factor for vine in this area **(Table 3.2)**.

The structural stability of the soils in the Montalcino's vineyards is overall medium-low. Since very acidic soils are not present to a significant extent in sodium content, the cause of the modest structural stability is probably to be found in the not particularly high content of organic substance and in the frequent tillage to which agricultural soils are subject **(Table 3.2)**.

From a chemical point of view, the average organic C content in the surface layer (0-30 cm) of the soil is equal to 0.95%, therefore classifiable as medium. The soils have on average a weakly alkaline reaction (pH=7.7).

The cation exchange capacity (CSC), the quantity of hydrogen cations plus metal cations that a soil can fix on mineral and organic colloids, is moderately high (19.7 meq/100 g); we are therefore in the presence of soils that have an adequate nutrient retention capacity **(Table 3.3)**. The saturation rate in bases, expressed by the percentage value of the ratio between the sum of the exchangeable metal cations and the CSC, is on average very high (100%). Electrical conductivity represents the indirect measurement of the concentration of dissolved salts in the circulating soil solution. On average, the Montalcino's vineyards soils have a negligible level of salinity (0.14 ds m-1). Exchangeable calcium is present in high quantities (23.4 meq/100 g) **(Table 3.3)**. Total nitrogen is present in low quantities (N=0.51 g kg-1); 75% of the soils have an average total nitrogen content of less than 1.0 g.kg-1.

The soils of the Montalcino's vineyards are rich in total limestone, a parameter through which the total carbonate (CaCo3) content of the soil is quantified. The average figure is 14.2%, which corresponds to soils rated as very calcareous **(Table 3.3)**. The exchangeable Mg content is high on average (Mg=2.3 meq/100g), and the average exchangeable K content is high (0.68 meq/100g), in fact, supply of exchangeable K can be expressed by knowing about textural of characteristics of soils, for instance clay requires higher K contents to ensure adequate nutrient availability to the crops.

Finally, The Na content (Na=0.29 meq/100g) does not cause particular concerns; in fact, over 90% of soils have normal levels of Na on the exchange complex (<1 meq/100g). The assimilable microelements (Fe, Mn, and Cu) show normal values and the soils can be classified as having an average content of these elements **(Table 3.3)**.

Table 3.1. statistics related to the stationary characteristics of the vineyard areas, Montalcino

	Min Value	Moderate Value	Max Value
Attitude (m)	100	276	500
Slope (%)	0	7.6	24
Exposure	45	218	338

Table 3.2. statistics related to the Physical and Hydrological characteristics of the vineyard areas, Montalcino

	Min Value	Moderate Value	Max Value
Useful Dept (cm)	3	94	140
Stoniness (%)	0	7.8	37
Skeleton	0	22.4	90
Clay (%)	24	33.5	49.3
Limestone (%)	21	33.1	48.1
Sand (%)	13.1	35.4	54
Internal drainage (class)	3	4	6
External drainage (class)	2	4	5
AWC (mm)	52	106	185
Density (g cm-3)	1.1	1.36	1.64
COLE (%)	0.21	4.37	7.33
Structural Stability(mm)	0.26	0.41	0.55

Table 3.3. statistics related to the Chemical characteristics of the vineyard areas, Montalcino

	Min Value	Moderate Value	Max Value
PH	7.3	7.7	8.2
C org (%)	0.27	0.95	1.2
CSC (meq/100g)	14.2	19.7	27.2
Saturation (%)	100	100	100
Cond.Electrical(ds m-1)	0.05	0.14	0.19
Na (meq/100g)	0.04	0.29	0.8
Calcare.tot (%)	0	14.2	41.1
Ca (meq/100g)	12.8	23.4	45.2
Mg (meq/100g)	0.7	2.3	5.7
K (meq/100g)	0.19	0.68	2.25
Mn (meq/100g)	9.4	9.5	9.6
Fe (meq/100g)	8.2	8.6	9
Cu (meq/100g)	2	3	4
N.tot (g.kg-1)	0.01	0.51	1

Having analyzed the soil characteristics in numerous vineyards throughout the Montalcino region, we now turn our attention to a more intricate analysis of the soil properties within a particular vineyard. This specific vineyard is located in Sant' Angelo in Colle and is known as Poggione vineyard (47°61'67"N 17°00'75"E) **(Figure 3.12)**.

In terms of functional characteristics, there is an absence of erosion, characterized by low surface flow and efficient internal drainage. Additionally, the soil boasts a moderately high useful depth, spanning from 50cm to 100cm, and a water-holding capacity ranging between 100mm and 150mm **(Table 3.4)**. Given that the maximum useful depth extends to 1 m, we will delve into the analysis of soil characteristics in three distinct sections:

At the depth of 30cm (0-30cm), soil is identified on surfaces of small aggregates. The framework is thin with coarse gravel (20-76 mm), and angular form. The estimated texture is clay, featuring a large, well-developed subangular polyhedral structure. This texture is robust, exceptionally adhesive, and notably plastic, exhibiting a moderately high hydraulic conductivity.

Fine pores (0.5-1 mm) are frequent, and there are a few small (6-20 mm) calcium carbonate concretions (CaCo3). The soil demonstrates noticeable effervescence, with a reaction estimate indicating weak alkalinity, specifically a pH range of between 7.4 and 7.8.

At the depth of 60 cm(30cm-60cm), soil is identified on the surfaces of small aggregates. The skeleton remains thin, with coarse gravel (20-76 mm), an angular shape, either moderately weathered or slightly altered. The texture remains clay, featuring a large, strongly developed subangular polyhedral structure, and the soil demonstrates a moderately high hydraulic conductivity. Fine pores (0.5-1 mm) remain common, and both fine (0.5-1 mm) and large (>76 mm) soft calcium carbonate concentrations become common. Very small (3-5 mm) calcium carbonate concretions are also common. The soils also remain noticeable effervescence, with a reaction estimate indicating weak alkalinity, specifically a pH range of between 7.4 and 7.8.

Table 3.4. statistics related to the Chemical, Physical, and Hydrological characteristics of the Poggione vineyard, Montalcino

Depth (cm)	**Attitude (m)**	**Slope (%)**	**Exposure**	**Stoniness (%)**	**Lime Stone (%)**	**Clay (%)**	**CaCO3 (%)**	**C (%)**	**PH**	**N.tot (g.kg-1)**	**AWC (mm)**	**Cond.Ele (ds m-1)**	**Useful Depth (cm)**
0-100	255	2-4	18	0,50	24,29	39,44	7.7,31	0.19,0.95	7.3,8	1	100,150	0.13,0.14	50,100

Figure 3.12. vineyard's soil, Poggione

At the depth of 100 cm(60cm-100cm), soils remain on the surfaces of small aggregates. The skeleton is thinly distributed, with coarse gravel (20-76 mm) showing an angular shape, and moderately altered. Abundant content of the stone type (250-600 mm) emerges, featuring a sub-rounded shape and displaying minimal alteration. The texture remains clay, featuring a large, strongly developed subangular polyhedral structure, and the soil demonstrates a moderately high hydraulic conductivity. Fine pores (0.5-1 mm) remain common, and both very small (3-5mm) and small (6-20 mm) soft calcium carbonate concentrations become common. The soils also remain noticeable effervescence, with a reaction estimate indicating weak alkalinity, specifically a pH range of between 7.4 and 7.8.

In the following chapters, we will see how after using geophysical methods, soil characteristics information can be useful for detailed analysis of the subsurface.

3.4. Grape Varieties

In Poggione vineyard, cultivate a variety of different grapes for wine making, some of which are endemic to the area. These grapes offer a diverse range of possible combinations to make the wines that they are known for, creating wines with their own taste and quality **(Table 3.5)**.

Table 3.5. different grape varieties cultivated by the Poggione vineyard, divided into red wines and white wines, and rose wine

Wine	Wine Type	Grape
Brunello Di Montalcino	Red Wine	Sangiovese
Rosso Di Montalcino	Red Wine	Sangiovese
Rosso Di Toscana	Red Wine	Sangiovese, Merlot
Bianco Di Toscana	White Wine	Chardonnay
Lo Sbrancato	Rose Wine	Sangiovese
Vin Santo Sant' Antimo	Rose Wine	Trebbiano and Malvasia
Moscadello di Montalcino	White Wine	Moscato
Grappa Di Brunello	White Wine	Sangiovese

The grape varieties that are found within the wines produced by the Poggione vineyard are Sangiovese, Chardonnay, Malvasia del Chianti, Merlot, Trebbiano Toscano. Their characteristic and cultivation areas are described below [20]:

- **Chardonnay**: Chardonnay cultivation has undergone a significant increase in its planted area, marking a notable expansion from 1982 to 2010. By the latter year, an estimated 20,000 hectares were dedicated to the cultivation of Chardonnay grapes. The grapes themselves are identifiable by their moderate, round size, accompanied by a skin that

ranges in thickness from thin to medium. Notably, the skin displays a characteristic average pruinoise texture, which plays a pivotal role in defining the unique attributes of this particular grape variety. The ultimate outcome of this cultivation effort is the production of a captivating wine, distinguished by its alluring amber-yellow color, a visual testament to the distinct characteristics of Chardonnay grapes.

- **Malvasia del Chianti:** The cultivation of Malvasia del Chianti, specifically the Malvasia Bianca lunga variant, has undergone a consistent reduction in cultivated land over the years, dwindling from 17,500 hectares in 1970 to a mere 2,200 hectares by 2010. This decline in planted area reflects a shifting trend in viticulture practices over the decades. The Malvasia Bianca long grape itself is characterized by a medium to small size, with a diameter ranging between 11 to 13 millimeters. The grapes take on a spherical shape, and their skin exhibits a pruinose texture, imparting a distinctive quality to the grape. The color of the skin is a greenish light gold, contributing to its visual appeal. In terms of skin resistance, Malvasia Bianca lunga possesses a rather resilient outer layer, although it falls slightly short of the resistance observed in the Trebbiano variety. The ripening process of these grapes unfolds in the latter part of September, extending up to the 15th of October, a critical period that influences the grape's flavor profile and overall quality.

- **Merlot:** Merlot has experienced a decline in cultivated area since 1970, diminishing from a little over 50,000 hectares to approximately 28,000 hectares by 2010. This shift in acreage illustrates a noteworthy transformation in the viticultural landscape over the four decades. The Merlot grape itself is characterized by a moderate size, with berries falling into the medium category. The skin thickness is also of a medium degree, contributing to the grape's overall composition. The distinctive feature of Merlot lies in its berry color, presenting a shade of blue-black that defines its visual identity. The ripening process for Merlot grapes is a crucial phase in their development, typically taking place towards the end of September and extending into the early days of October. This period is significant as it directly influences the flavor profile, tannin structure, and aromatic characteristics of the resulting wine.

- **Sangiovese:** Sangiovese has undergone a notable reduction in cultivated areas since 1982, where the expansive vineyards covered over 101 thousand hectares. By 2010, this expanse had decreased to approximately 71.5 thousand hectares across all of Italy. The Sangiovese grape, central to the production of Chianti wine, exhibits distinctive characteristics. Falling within the medium-size category, with a diameter ranging from 12 to 15 millimeters, the grape features a black-purple color reminiscent of an ellipsoid **(Figure 3.13)**. The skin of the Sangiovese grape is described as pruinose, contributing a textured quality to its appearance. The maturation process unfolds in the latter part of September, extending up to the middle of October, marking a critical phase in the grape's development. Within the region of Tuscany, Sangiovese takes the lead as the most cultivated grape variety, representing a significant portion, over 50%, of all grapes grown in Italy.

- **Trebbiano Toscano**: Originating in the attractive region of Tuscany, Trebbiano Toscano stands as a testament to the rich viticultural heritage of the area. The grapes of Trebbiano Toscano, typically medium-sized with a diameter ranging from 13 to 15 millimeters, showcase a distinctive green hue that characterizes the grape variety. The shape of the grape is notably uniform, round, and pruinose skin. Maturation of the grape usually occurs within the first half of October.

Figure 3.13. Sangiovese grape, Poggione vineyard, Sant' Angelo in Colle, Montalcino

4. Geophysical Methods

Applied geophysics serves the purpose of understanding what lies beneath the Earth's surface, delving into the geology, geological structures, groundwater, contamination, and human artifacts. The exploration of conditions beneath the Earth involves measuring, analyzing, and interpreting physical fields on the surface. This process relies on mapping variations in physical properties both laterally and vertically, using non-invasive technologies to remotely sense these variations.

Geophysical prospection methods mainly fall into two groups: active and passive. In the active approach, a source energizes the ground, and receivers detect resulting variations in physical

quantities. Conversely, in the passive method, variations in intrinsic physical quantities are observed without the need for artificial energization.

Traditionally, geophysical technologies have been employed for exploring economic materials like groundwater, metals, and hydrocarbons. However, with the increasing recognition of the consequences of industrialization and environmental neglect, there has been a shift towards sustainable development and a heightened awareness of natural conservation. This shift has led to the adoption of methodologies and technologies to address the growing need for environmental assessment, monitoring, and remediation.

In practical applications, active geophysical techniques are utilized for soil characterization during fieldwork. One such method is electrical resistivity tomography (ERT), which will be explored in the following chapter. Additionally, the OHM mapper will be introduced. Each method begins by explaining the physics behind the method, followed by details about the instruments used and the field configurations. The conclusion of each method provides a description of data analysis and processing techniques.

5. Theory

5.1. Electrical Resistivity Survey

Electrical resistivity surveys play an important role in assessing the electrical resistance of the ground beneath us. This is achieved through measurements taken on the surface of the ground, providing valuable insights into the subsurface’s resistance. The resistance is intricately linked to various Earth elements, including minerals, fluids, porosity (the space between particles), and the water content within the rock.

For an extensive period, electrical surveys have been in existence, serving multiple purposes such as assessing groundwater, prospecting for minerals in mining operations, and gaining insights into the Earth's composition for construction projects. Recently, there has been a shift in their application, with these surveys being employed to monitor and track environmental conditions.

The aim of this chapter is to provide a brief description of this methodology with the definition of some fundamental concepts.

5.2. ERT

Electrical Resistivity Tomography (ERT) stands out as a reliable geophysical method, offering valuable insights into the electrical properties of a surveyed area. This method relies on a four-electrode array, commonly known as a quadrupole. Within this arrangement, two electrodes, designated as potential points, measure voltage, while the other two electrodes apply an electric field to the ground.

ERT has proven its effectiveness through successful applications in imaging subsurface structures and characterizing diverse aspects such as groundwater, faults, contaminant plumes, and various environmental issues. Often referred to as Hydrogeophysics, ERT reflects its significant reliance on variations in water content and water chemistry. The technique delves into the spatial distribution of the electrical resistivity of the ground, providing a comprehensive understanding of the subsurface conditions.

5.2.1. Theoretical background

ERT operates as a direct current (DC) electric method, and its foundation lies in Ohm's law:

$$\Delta V = IR \tag{5.1}$$

where ΔV is the electric potential difference [V], I is the injected current [A], and R is the resistance [Ω] given by the soil to the current flow. This last parameter is related not only to electrical features but also to material and geometric properties. In fact, if we consider a current flow through a cylindrical conductor with length L [m] and area A [m2], for the second Ohm's law we have **(Figure 5.1)**:

$$\rho = \frac{R \times A}{L} \quad (5.2)$$

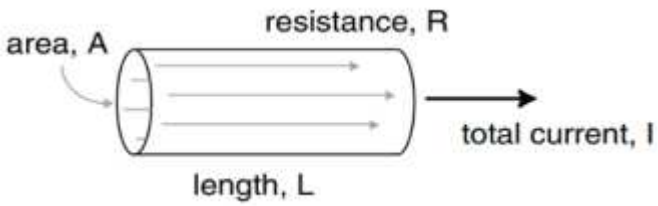

Figure 5.1. Definition of resistivity

where ρ is the electrical resistivity [Ωm]. Electrical resistivity can also be defined as 1/σ, where σ is the electrical conductivity [S/m] of the material, a measure of the ability of a material to sustain long-term electric current flow **(Figure 5.1).**

5.2.2. Electrical properties of rocks

Electrical current moves through the Earth at shallow depths using two primary methods: electronic conduction and electrolytic conduction. In electronic conduction, the current flows through free electrons, commonly found in metals. On the other hand, electrolytic conduction occurs when ions in groundwater carry the current. In surveys related to the environment and engineering, electrolytic conduction tends to be more prevalent. Electronic conduction becomes crucial when conductive minerals like metal sulfides and graphite are present, particularly in mineral surveys [21].

The resistivity, or the resistance to electrical flow, of common rocks, soil materials, and chemicals is displayed in **(Figure 5.2)**. Igneous and metamorphic rocks typically exhibit high resistivity values, influenced by factors such as the degree of fracturing and the percentage of fractures filled with groundwater. This variability in resistivity, ranging from about 1000 to 10 million Ω·m, proves useful in identifying fracture zones and weathering features in engineering and groundwater surveys. In contrast, sedimentary rocks, being more porous with higher water

content, generally display lower resistivity values compared to their igneous and metamorphic counterparts, ranging from 10 to about 10000 Ω·m.

Unconsolidated sediments, characterized by even higher porosity, exhibit even lower resistivity values, ranging from about 10 to less than 1000 Ω·m. The resistivity value here is influenced by porosity and clay content. Clayey soil typically has lower resistivity than sandy soil. However, there is an overlap in resistivity values among different rock and soil classes due to factors such as porosity, water saturation, and salt concentration.

Increasing of salinity, porosity φ, and temperature T trigger a rising in electrolytic process and directly affect the bulk electrical conductivity. Interconnected and saturated pores represent pathways for electrical conduction, owing to the presence of dissolved ions in the pore-fluid solution. The electrical conduction is assumed to be through the fluids filling the pores of the rock:

$$\rho = F\rho W = \frac{a}{\phi m \times S n}\rho W \qquad \text{(Archie's law)} \qquad (5.3)$$

where ρ and ρ_w are respectively the bulk resistivities of the medium and the fluid; φ the porosity; a, m and n empirical constants (m = cementation exponent 1.3<m<2.4, 0.5<a<1 generally ≅ 1, n≅ 2), F the formation factor linked to porosity and pore tortuosity, always >1; S the water saturation Vwater/Vpores (0 ≤ S ≤ 1).

Groundwater resistivity varies from 10 to 100 Ω·m, depending on dissolved salt concentration. Notably, seawater has a low resistivity (about 0.2 Ω·m) due to its high salt content. This makes resistivity a useful method for mapping the interface between saline and fresh water in coastal areas.

Metallic sulfides (such as pyrrhotite, galena and pyrite) have typically low resistivity values of less than 1 Ω·m. Most oxides, such as hematite, do not have a significantly low resistivity value. One of the exceptions is magnetite.

Metals, such as iron, have extremely low resistivity values. Chemicals that are strong electrolytes, such as potassium chloride and sodium chloride, can greatly reduce the resistivity of ground water to less than 1 Ω·m even at fairly low concentrations. The effect of weak electrolytes, such as acetic acid, is comparatively smaller. Hydrocarbons, such as xylene, typically have very high resistivity values. However, in practice the percentage of hydrocarbons in a rock or soil is usually quite small, and might not have a significant effect on the bulk resistivity.

Having a grasp of resistivity values offers a potent tool across various domains, ranging from recognizing geological features to evaluating environmental issues. In the upcoming chapters, we'll delve into how leveraging the electrical properties of rocks, coupled with the application of geophysical methods like ERT and Ohm mapper, proves beneficial for scrutinizing the subsurface of our case study.

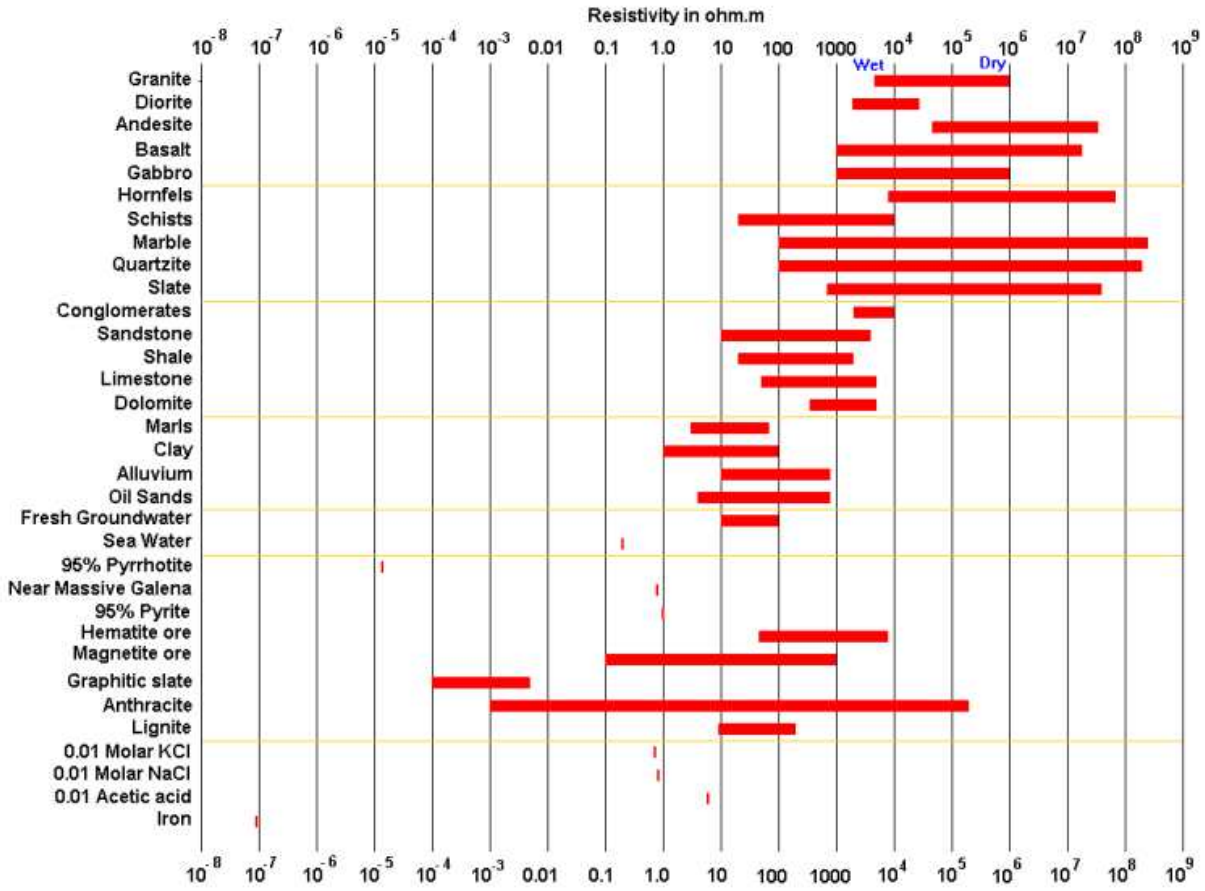

Figure 5.2. The resistivity of rocks, soils and minerals

5.2.3. Physics

Combining equations **(5.1)** and **(5.2)** in an infinitesimal way, we have:

$$\Delta I = \frac{\Delta S}{\Delta L} \cdot \frac{-\Delta V}{\rho} \quad , \quad \frac{\Delta I}{\Delta S} = \frac{-\Delta V}{\Delta L} \cdot \frac{1}{\rho} \quad , \quad J = \frac{E}{\rho} \tag{5.4}$$

where E is the electric field intensity vector [V/m] and J is the current intensity vector [A/m2].

Using electrical conductivity, we can write the most common:

$$J = \sigma E \tag{5.5}$$

Since electrostatic field are conservatives, electric field can be expressed as the gradient of the scalar field of potential V:

$$E = -\nabla V \tag{5.6}$$

and replacing this into the equation (5.5), we get the Ohm's law (5.1) in differential way:

$$J = -\sigma \nabla V \tag{5.7}$$

As stated before, a fundamental principle for the DC electrical methods is the charge conservation, expression of stationarity of electrical flow. Generally, this principle is written in differential way:

$$\nabla \cdot J = 0 \tag{5.8}$$

where ∇ = ∂/∂x, ∂/∂y, ∂/∂z indicates the divergence of the vector. Replacing equation **(5.7)** in (5.8) we get the potential distribution in stationary conditions:

$$\nabla \cdot (-\sigma \nabla V) = 0 \tag{5.9}$$

$$\frac{\partial}{\partial x}(\sigma \boldsymbol{x}(x,y,z)\frac{\partial V}{\partial x}) + \frac{\partial}{\partial y}\left(\sigma \boldsymbol{y}(x,y,z)\frac{\partial V}{\partial y}\right) + \frac{\partial}{\partial z}\left(\sigma \boldsymbol{Z}(x,y,z)\frac{\partial V}{\partial z}\right) = 0 \tag{5.10}$$

This latter full form expression shows the possible heterogeneity and anisotropy of σ.

Given a homogeneous system, the partial derivatives of σ cancel each other:

$$\sigma \boldsymbol{x}(\frac{\partial 2_V}{\partial x 2}) + \sigma \boldsymbol{y}(\frac{\partial 2_V}{\partial y 2}) + \sigma Z\left(\frac{\partial 2_V}{\partial z 2}\right) = 0 \tag{5.11}$$

and assuming it even isotropic (σ=σx=σy=σz), we can write:

$$\sigma\left(\frac{\partial 2_V}{\partial x 2} + \frac{\partial 2_V}{\partial y 2} + \frac{\partial 2_V}{\partial z 2}\right) = 0 \tag{5.12}$$

That is equivalent to the Laplace's equation:

$$\nabla 2V = 0 \tag{5.13}$$

Laplace's equation generally represents the diffusion by potential gradient through a homogeneous and isotropic medium.

5.2.4. Single electrode

Considering our interest, it proves beneficial to rephrase Laplace's equation in spherical coordinates:

$$\left(\frac{\partial 2V}{\partial r2} + \frac{2}{r} \cdot \frac{\partial V}{\partial r}\right) = 0 \qquad (5.14)$$

This approach facilitates the examination of a single electrode case, positioned at the origin of the coordinate system (r=0), where the current I is introduced into a uniform space with resistivity ρ. The generic solution can be obtained:

$$\frac{\partial}{\partial r}\left(r2\frac{\partial V}{\partial r}\right) = 0 \qquad (5.15)$$

$$\rightarrow \left(r2\frac{\partial V}{\partial r}\right) = constant = C1$$

$$\rightarrow c2 - \frac{C1}{r} = V$$

Where C_1 and C_2 represent constants established by boundary conditions. It is a standard practice to set the condition V=0 as the distance r extends to infinity. Simultaneously, using spherical symmetry with the electrode at the origin, we can express the current J as a function of r:

$$V(r \rightarrow \infty) \rightarrow C2 = 0 \qquad (5.16)$$

$$I = 4\pi r2J \rightarrow I = -4\pi r2\sigma\frac{\partial V}{\partial r} \rightarrow I = -4\pi r2\sigma\frac{C1}{r2} \rightarrow C1 = -\frac{I\rho}{4\pi} \qquad (5.17)$$

$$V(r) = \frac{I\rho}{4\pi r} \qquad (5.18)$$

Therefore, it is possible to transcribe this result in the event that the electrode is placed upon the surface of a homogeneous half space **(Figure 5.3)**. In this more physically realistic case, the current I is distributed upon only half of the previous volume and the current density J is double:

$$V(r) = \frac{I\rho}{2\pi r} \tag{5.19}$$

$$J = \sigma E = \frac{-dV}{dr} \cdot \frac{1}{\rho} = \frac{I}{2\pi r 2} \tag{5.20}$$

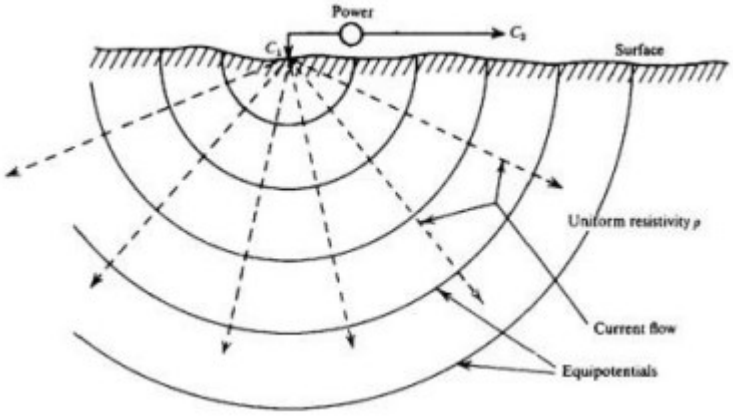

Figure 5.3. Electric field for a single electrode charge in a half-space

5.2.5. Multiple electrodes

In the electrical resistivity tomography (ERT) technique, one couple of electrodes (C_1, C_2) is utilized for injecting current, while another couple of electrodes (P_1, P_2) is used for measuring potential difference. When considering electrodes positioned on the surface of a homogeneous half-space **(Figure 5.4)**, the current follows a radial path through a hemisphere with a radius of 'r' and a surface area of $2\pi r^2$.

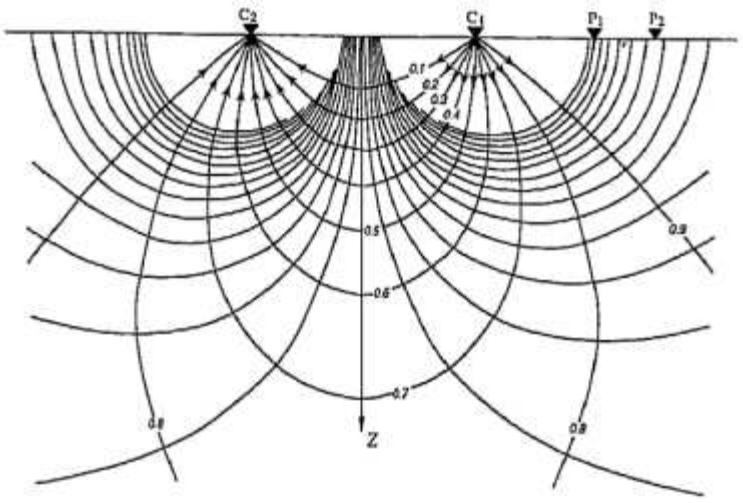

Figure 5.4. Current (C) and potential (P) electrodes placed on the surface of a homogeneous half-space and distribution of the current and potential lines

Information about spatial changes in subsurface electrical properties can be obtained by conducting measurements using hundreds of electrodes. The difference of potential can be easily written by the effect overlapping:

$$VP1 = \frac{I\rho}{2\pi r1} + \frac{-I\rho}{2\pi r2} \quad , \quad VP2 = \frac{I\rho}{2\pi r3} + \frac{-I\rho}{2\pi r4} \tag{5.21}$$

from which we obtain the measured ΔV:

$$\Delta V = \frac{I\rho}{2\pi} + \left[\left(\frac{1}{r1} - \frac{1}{r2}\right) - \left(\frac{1}{r3} - \frac{1}{r4}\right)\right] \tag{5.22}$$

To distinguish between the resistance arising from the medium and the contact resistance, which is influenced by the diverse electrical properties of both the electrodes and the ground, employing four electrodes is necessary **(Figure5.5)**. The electrodes exhibit electronic conductivity, whereas the ground acts as an ionic conductor. If only two electrodes were used for measuring current and potential, it would be impossible to differentiate between the two contributions and eliminate the contact resistance, which depends on the current intensity flowing through.

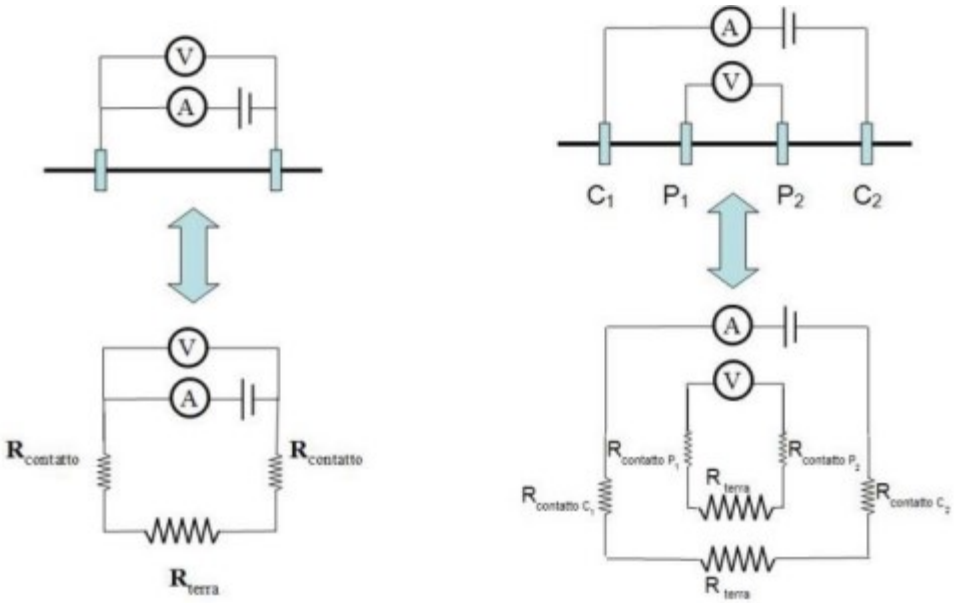

Figure 5.5. DC-resistivity dipole - on the left - and quadrupole - on the right

Previously, we operated under the assumption of the complete homogeneity of the medium where the electric field is produced. Nevertheless, a geological cross-section might exhibit variations and sets of lithologically defined interfaces that cause the current lines to deviate through diffraction. These lines will adjust to follow paths of minimum resistance in accordance with Fermat's principle. If we examine a two-layer domain, we can observe how the lines of current flow are altered due to both vertical and lateral changes in subsurface resistivity **(Figure 5.6)**.

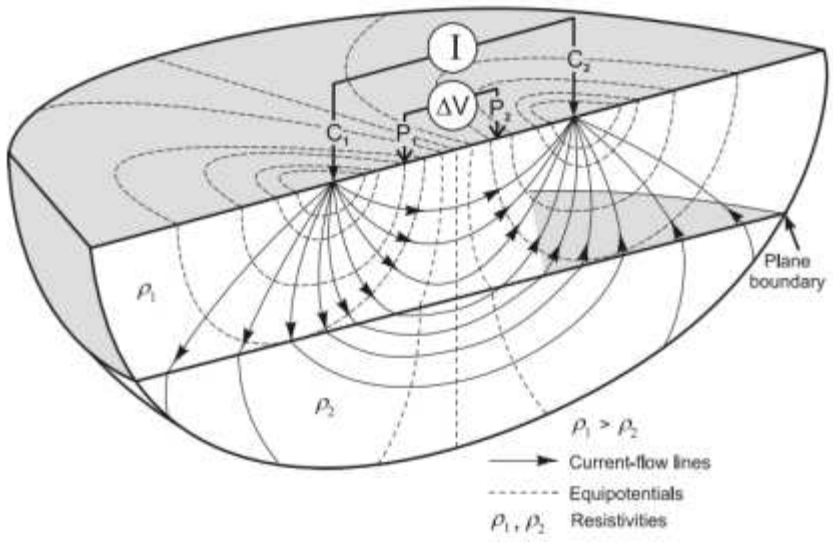

Figure 5.6. Principle of resistivity measurement with a four-electrodes array in a nonhomogeneous system.

The heterogeneity distribution of resistivity within the Earth enables us to modify equation **(5.18)** to find an apparent resistivity (ρ_a). This apparent resistivity is construed as the resistivity that would be observed if we were dealing with a flat, homogeneous Earth domain:

$$\rho a = \frac{K\Delta V}{I} \qquad (5.23)$$

The real resistivity values are determined through the inversion process that will be described later. Consider that ρ_a can be written as a product of the measured Earth impedance $Z = \Delta V/I$ and a geometric factor K that depends only on the chosen electrodes array:

$$Z = \frac{\Delta V}{I} \tag{5.24}$$

$$K = 2\pi\left[\left(\frac{1}{r1} - \frac{1}{r2}\right) - \left(\frac{1}{r3} - \frac{1}{r4}\right)\right] - 1 \tag{5.25}$$

5.2.6. Electrode arrays

An electrode array is a geometric configuration describing the relative position of current and potential electrodes in a quadrupole **(Figure 5.7)**. Several configurations are available, and each should be chosen according to the objective of the study, the depth of investigation, site access, and instrument limitations **(Figure 5.8)**.

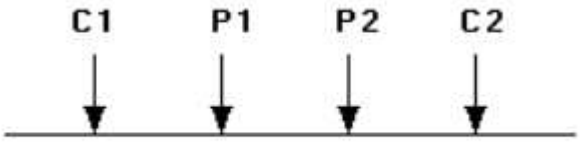

Figure5.7. A conventional array with four electrodes to measure the subsurface resistivity

Key features include signal intensity, as well as lateral and vertical resolution. These aspects are directly influenced by the electrode spacing established by the array. The greater spacing between electrodes, the deeper the penetration of current lines, but with lower resolution. Consequently, shorter electrode spacing limits current paths to the upper portion of the subsurface domain, potentially neglecting exploration of the lower layer.

In general, the investigation depth is set at 1/5 of the length of the array, but it is also strongly influenced by the cable length, by the power supply and by the electrical characteristics of the investigated domain.

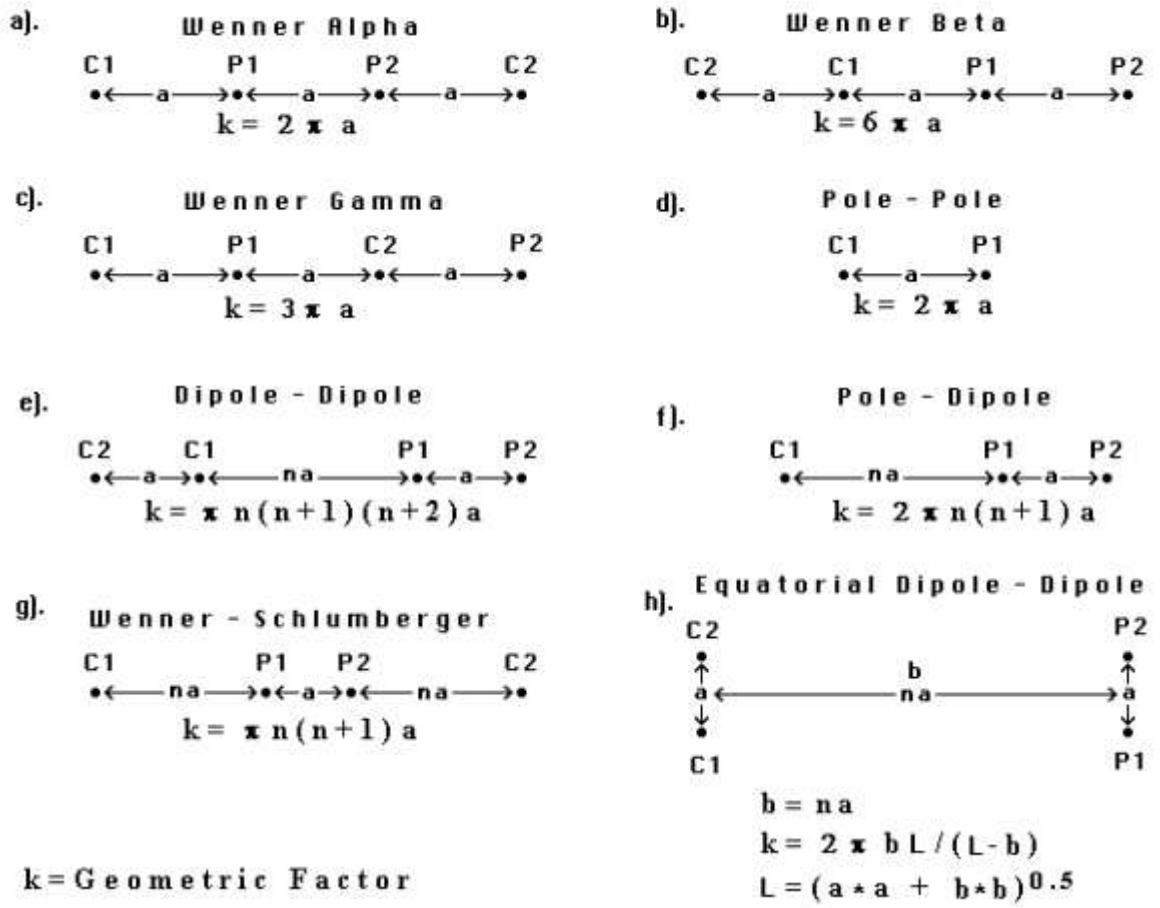

Figure 5.8. Common arrays used in resistivity surveys and their geometric factors.

5.2.7. Equipment

The SYSCAL Pro Switch is a versatile electrical resistivity meter that consolidates a transmitter, a receiver, and a switching unit into a single housing **(Figure 5.9)**. It is powered by a 12V battery. Automatic measurements (output voltage, stacking number, quality factor) are executed after the operator selects limit values and are stored in the internal memory. The output specifications include 800V in switch mode, 1000V in manual mode, 2.5A, and 250W with the internal converter and a 12V battery. Utilizing multi-core cables, the SYSCAL Pro Switch controls a set of electrodes connected in a line or multiple lines. The standard number of electrodes (24, 48, 72, 96, 120) can

be expanded through Switch Pro units for 2D or 3D ground images. The system's ten channels enable up to 10 readings simultaneously, ensuring high efficiency.

In the chapter on data acquisition, we will provide a detailed explanation of how to utilize the SYSCAL Pro resistivity meter for acquiring data in our specific case study.

Figure 5.9. SYSCAL PRO Resistivity meter

5.3. OHM mapper

The Geometrics OhmMapper is a capacitively-coupled resistivity meter that measures the electrical properties of rock and soil without cumbersome galvanic electrodes used in traditional resistivity surveys. A simple coaxial cable array with transmitter and receiver sections is pulled along the ground either by a single person or by a small all-terrain vehicle. Data acquisition is many times faster than DC resistivity **(Figure 5.10)**. Multiple passes with the OhmMapper, or a single pass with multiple receivers at different transmitter-receiver spacings, permit 2D and even 3D electrical surveying at a fraction of the time of resistivity or electromagnetic methods. Data acquisition is near-continuous, providing maximum resolution.

Figure 5.10. Ohm mapper instrument

5.3.1. Theoretical Background

One of the primary challenges faced in performing resistivity surveys involves the time-consuming task of inserting electrodes into the ground. This process hinders the swift creation of multiple resistivity profiles in the designated area of investigation. However, a solution to this issue is readily available through the application of the OhmMapper.

The OhmMapper operates on the principle of capacitively coupled electrodes, a departure from the conventional galvanic georesistivimeters that employ conductive pickets. Ground energization is achieved using a pair of antennas, one serving as a transmitter and the other as a

receiver, operating at a frequency of 16.5 kHz. As these antennas are dragged across the terrain, they enable data acquisition at a rate of one reading per second. Beyond its swift investigation capabilities, the instrument's unique feature lies in its absence of disturbances arising from ground-peg contact resistances. This attribute renders the OhmMapper suitable for high-resistivity terrains or locations where electrode placement is impractical, such as on asphalt or historical pavements.

The instrument adopts the dipole-dipole configuration, a methodology that, when combined with the dense data acquisition, facilitates the generation of high-resolution resistivity profiles. With the OhmMapper, not only can resistivity maps be created at different depths, but the integration of these maps allows for the development of detailed 3D reconstructions of the subsoil.

Despite its merits, the instrument does have limitations. The maximum survey depth achievable is 15 meters, a common constraint associated with dipole-dipole arrays. This limitation stems from the signal intensity diminishing with the cube of the factor "n," where "n" represents the ratio between the distance separating the two antennas and the length of the antennas themselves. Additionally, the dipole-dipole spread is highly sensitive to horizontal changes in resistivity. Consequently, while the instrument excels in identifying vertical structures such as anthropic walls, dykes, and cavities, it is less suited for studying horizontal structures like sedimentary levels. These limitations, however, are not particularly problematic in agronomical applications.

5.3.2. Equipment

The setup of the OhmMapper entails arranging the transmitter at the extremity of the array, creating a distance from the receiver using a non-conductive cord whose length is proportionate to that of the antennas. Before reaching the receiver, a stabilizing optical fiber and a grounding weight precede it, enhancing the antenna's contact with the ground **(Figure 5.11)**. The entire

system establishes a connection with a console that is securely fastened to the user through a harness, facilitating deliberate and gradual movement.

In the configuration process, attention is given to the careful placement of the transmitter and receiver components, each with its specific role in optimizing signal stability and accuracy **(Figure 5.12)**. The non-conductive cord serves a crucial purpose, ensuring that the transmitter and receiver maintain an appropriate separation. This separation is not arbitrary but is meticulously determined, being directly proportional to the length of the antennas. The significance of this precision lies in the reliable transmission and reception of signals, contributing to the overall effectiveness of the OhmMapper.

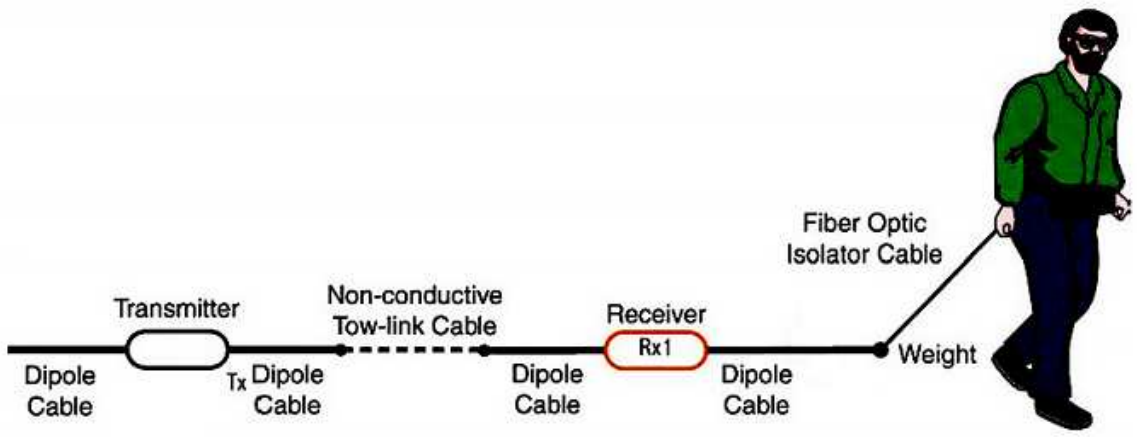

Figure 5.11. Ohm mapper configuration

The receiver is equipped with additional features to enhance its functionality. An optical fiber is strategically placed before the receiver, serving the purpose of signal stabilization. This addition contributes to the accuracy of the measurements by minimizing signal interference and fluctuations. Furthermore, a weight is incorporated into the setup, positioned in a way that optimizes the antenna's adherence to the ground. This meticulous configuration ensures that the

instrument maintains consistent and reliable contact with the surveyed terrain, a critical factor in obtaining accurate resistivity measurements.

The connection of the entire system to a console through a harness underscores the importance of user mobility. This design choice allows the user to move at a deliberate and controlled pace, ensuring that data collection is systematic and comprehensive. The harness acts as a tether, physically linking the user to the instrument, creating a symbiotic relationship that is essential for a successful survey.

Figure 5.12. Ohm mapper instrument

5.4. Inversion Theory

In geophysical inversion, we seek to find a model that gives a response that is similar to the actual measured values. The model is an idealized mathematical representation of a section of the earth. The model has a set of model parameters that are the physical quantities we want to estimate from the observed data. The model response is the synthetic data that can be calculated from the mathematical relationships defining the model for a given set of model parameters. All inversion methods essentially try to determine a model for the subsurface whose response agrees with the measured data subject to certain restrictions. In the cell-based method used by the RES2DINV and RES3DINV programs, the model parameters are the resistivity values of the model cells, while the data is the measured apparent resistivity values. The mathematical link between the model parameters and the model response for the 2-D and 3-D resistivity models is provided by the finite-difference or finite-element methods.

In all optimization methods, an initial model is modified in an iterative manner so that the difference between the model response and the observed data values is reduced. The set of observed data can be written as a column vector y given by:

$$y = col(y1, y2, \ldots, ym) \tag{5.26}$$

where m is the number of measurements. The model response f can be written in a similar form:

$$f = col(f1, f2, \ldots, fm) \tag{5.27}$$

For resistivity problems, it is a common practice to use the logarithm of the apparent resistivity values for the observed data and model response, and the logarithm of the model values as the model parameters. The model parameters can be represented by the following vector:

$$q = col(q1, q2, \ldots, qn) \tag{5.28}$$

where n is the number of model parameters. The difference between the observed data and the model response is given by the discrepancy vector g that is defined by:

$$y = q - f \tag{5.29}$$

In the least-squares optimization method, the initial model is modified such that the sum of squares error E of the difference between the model response and the observed data values is minimized:

$$E = gTg = \sum_{i=1}^{n} \quad gi2 \tag{5.30}$$

To reduce the above error value, the following Gauss-Newton equation is used to determine the change in the model parameters that should reduce the sum squares error:

$$JTJ\Delta qi = JTg \tag{5.31}$$

where Δq is the model parameter change vector, and J is the Jacobian matrix (of size m by n) of partial derivatives. The elements of the Jacobian matrix are given by:

$$Jij = \frac{\partial fi}{\partial qj} \tag{5.32}$$

that is the change in the ith model response due to a change in the jth model parameter. After calculating the parameter change vector, a new model is obtained by:

$$qk + 1 = qk + \Delta qk \tag{5.33}$$

In practice, the simple least-squares equation (5.30) is rarely used by itself in geophysical inversion. In some situations, the matrix product J^TJ might be singular, and thus the least-squares equation does not have a solution for Δq.

Another common problem is that the matrix product J^TJ is nearly singular. This can occur if a poor initial model that is very different from the optimum model is used. The parameter change vector calculated using equation (5.30) can have components that are too large such that the new model calculated with (5.32) might have values that are not realistic. One common method to avoid this problem is the Marquardt-Levenberg modification to the Gauss Newton equation that is given by:

$$\left(JTJ + \lambda I\right)\Delta qk = JTg \tag{5.34}$$

where I is the identity matrix. The factor λ is known as the Marquardt or damping factor, and this method is also known as the ridge regression method. The damping factor effectively constrains the range of values that the components of the parameter change vector can Δq take. While the Gauss-Newton method in equation (5.30) attempts to minimize the sum of squares of the discrepancy vector only, the Marquardt-Levenberg method modification also minimizes a combination of the magnitude of the discrepancy vector and the parameter change vector. This method has been successfully used in the inversion of resistivity sounding data where the model consists of a small number of layers. However, when the number of model parameters is large, such as in 2D and 3D inversion models that consist of a large number of small cells, the model produced by this method can have an erratic resistivity distribution with spurious high or low resistivity zones. To overcome this problem, the Gauss-Newton least-squares equation is further modified so as to minimize the spatial variations in the model parameters (i.e., the model resistivity values change in a smooth or gradual manner). This smoothness constrained least-squares method has the following mathematical form:

$$\left({}_{J}T_{J} + \lambda F\right)\Delta q k = {}_{J}T_{g} - \lambda F q k \tag{5.35}$$

Where

$$F = {}_{\alpha}x_{C}xT_{C}x + \alpha y_{C}yT_{C}y + \alpha z_{C}zT_{C}z$$

(5.36)

C_x, C_y and C_z are the smoothing matrices in the x, y and z-directions. α_x, α_y and α_z are the relative weights given to the smoothness filters in the x, y and z directions.

Equation (5.34) also tries to minimize the square of the spatial changes, or roughness, of the model resistivity values. It is in fact an l_2 norm smoothness-constrained optimization method. This tends to produce a model with a smooth variation of resistivity values. This approach is

acceptable if the actual subsurface resistivity varies in a smooth and gradational manner. In some cases, the subsurface geology consists of a number of regions that are internally almost homogeneous but with sharp boundaries between different regions.

For such cases, the inversion formulation in (5.34) can be modified so that it minimizes the absolute changes in the model resistivity values. This can sometimes give significantly better results. Technically this is referred to as an l_1 norm smoothness constrained optimization method, or more commonly known as a blocky inversion method. A number of techniques can be used for such a modification. One simple method to implement an l_1 norm-based optimization method using the standard least-squares formulation is the iteratively reweighted least-squares method. The optimization equation in (5.34) is modified to:

$$(JTJ + \lambda FR)\Delta qk = JTRd\ g - \lambda\ FR\ qk$$

(5.37)

Where

$$FR = \alpha xRmCxTCx + \alpha yRmCyTCy + \alpha zRmCzTCz$$

(5.38)

where R_d and R_m are weighting matrices introduced so that different elements of the data misfit and model roughness vectors are given equal weights in the inversion process.

Equation (5.36) provides a general method that can be further modified if necessary to include known information about the subsurface geology.

6. Data Acquisition

6.1. 3D ERT

The general approach for ERT data acquisition consists of several electrodes placed along a straight line, which location and spacing are chosen according to the objectives of the survey. The measurement of a 3D takes place using a resistivity meter, which automatically switches between current and potential electrodes according to the chosen sequence thanks to a multiplexer.

This instrument, which sends the current to each single electrode planned for the test, measures and stores the resulting potential for each quadrupole. The electrodes are linked to the resistivity meter thanks to one or more multicore cables. For the ERT method, current injection is performed through the electrodes as positive and negative pulses to remove the self-potential effects in the signal. The voltage is only measured during the current injection, averaging the potential for a full period of the square wave **(Figure 6.1)**.

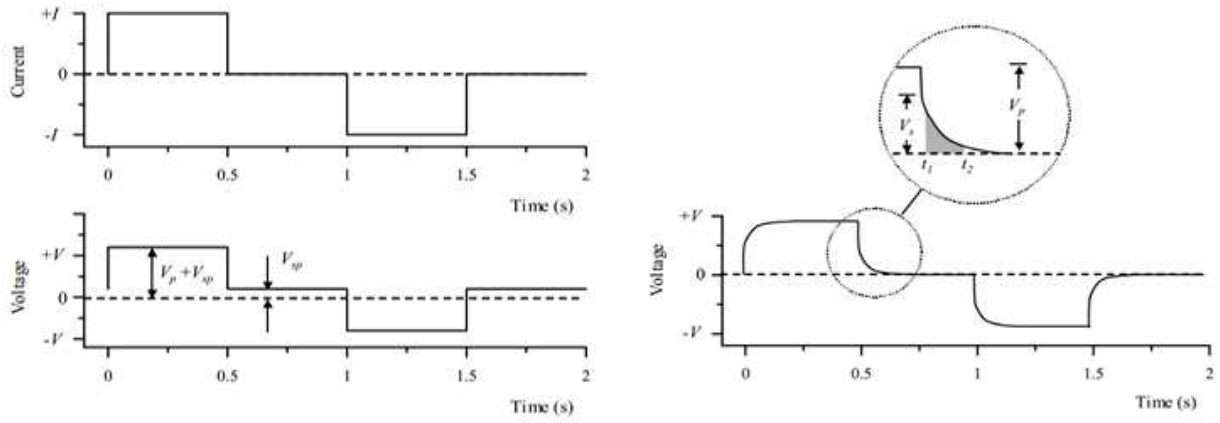

Figure 6.1. Fig. 4. 19, Left: Current injection as a square wave: alternating current and idealized voltage for field dc resistivity surveys, with primary voltage (Vp) and self-potential (Vsp) effects. Right-: Real voltage waveform for measurement of time-domain induced polarization.

ERT measurement was conducted in the part of poggione vineyard, close to Sant Angelo in Colle. In detail, our aim was to achieve the best image with high resolution and visualize soil characterization and assess water content in the subsurface. The data were collected along one

square profile of approximately 15m×15m, the resultant of 6 single lines oriented parallel to each other with 3m spacing **(Figure 6.2)**.

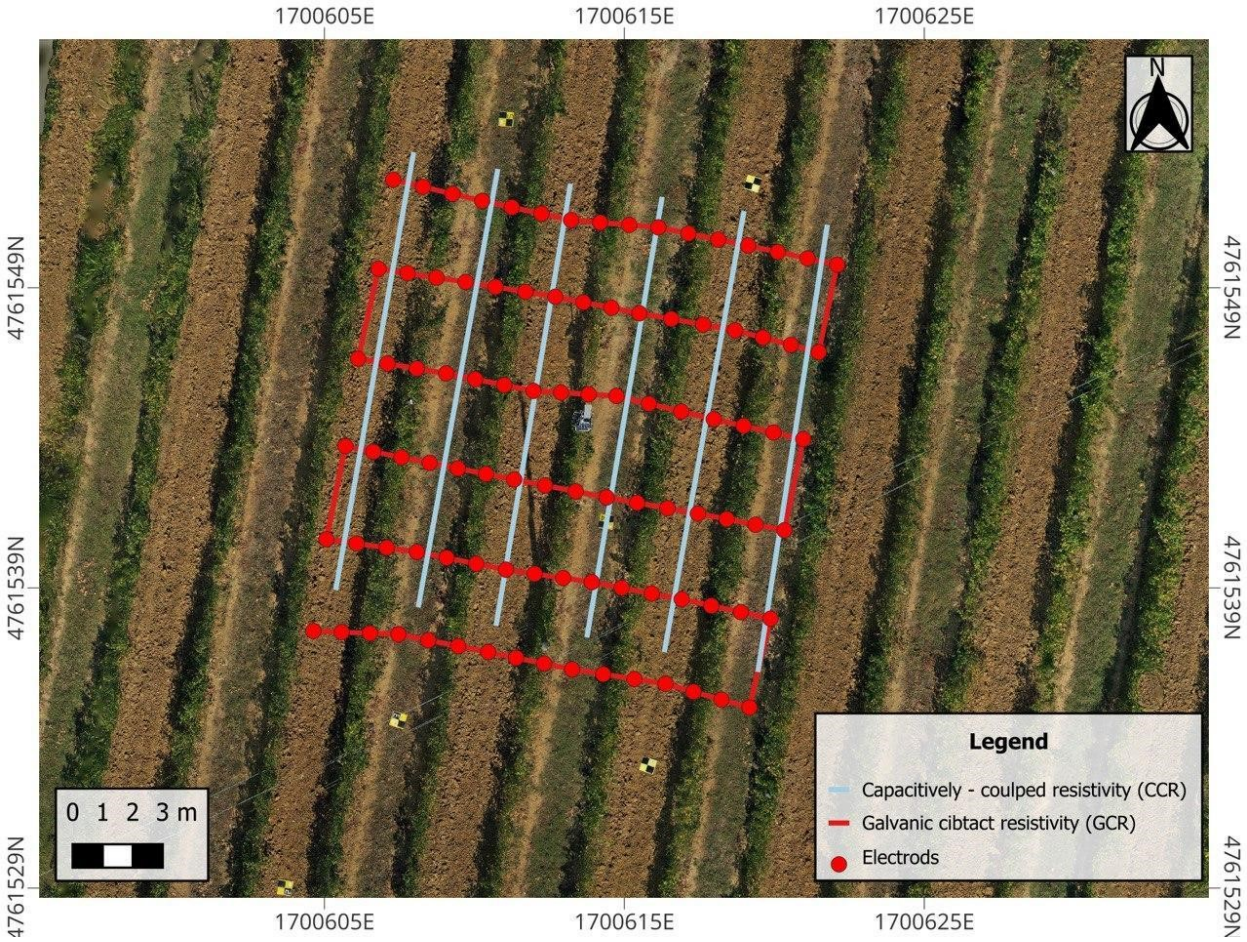

Figure 6.2. orthophoto of a specific part of area, which preformed 3D ERT and ohm mapper measurement

Figure 6.2. GPS Electrodes position in 3D ERT measurement and also 6 lines of ohm mapper which is perpendicular to 3D ERT measurement with QGIS software

For each line, we used multi-core cables and 16 stainless steel electrodes (total electrodes equal 96), connected to them with take-out jumpers, with a spacing of 1 m to enhance resolution but sacrificing the investigation depth, according to the shallow target **(Figure 6.3, 6.4)**.

Figure 6.3. putting electrodes with 1m spacing

Figure 6.4. ERT measurement in square profile, poggione vineyard

The data were acquired using a 10 channels resistivimeter Syscal Pro by IRIS Instruments, that made possible to collect resistivity measurement through 2A square-wave current injection and a pulse length of 500 ms **(Figure 6.5 ,6.6)**. The voltage decay was measured along 20 windows, having the same duration of 20 ms and starting after a delay of 50 ms after current shutoff.

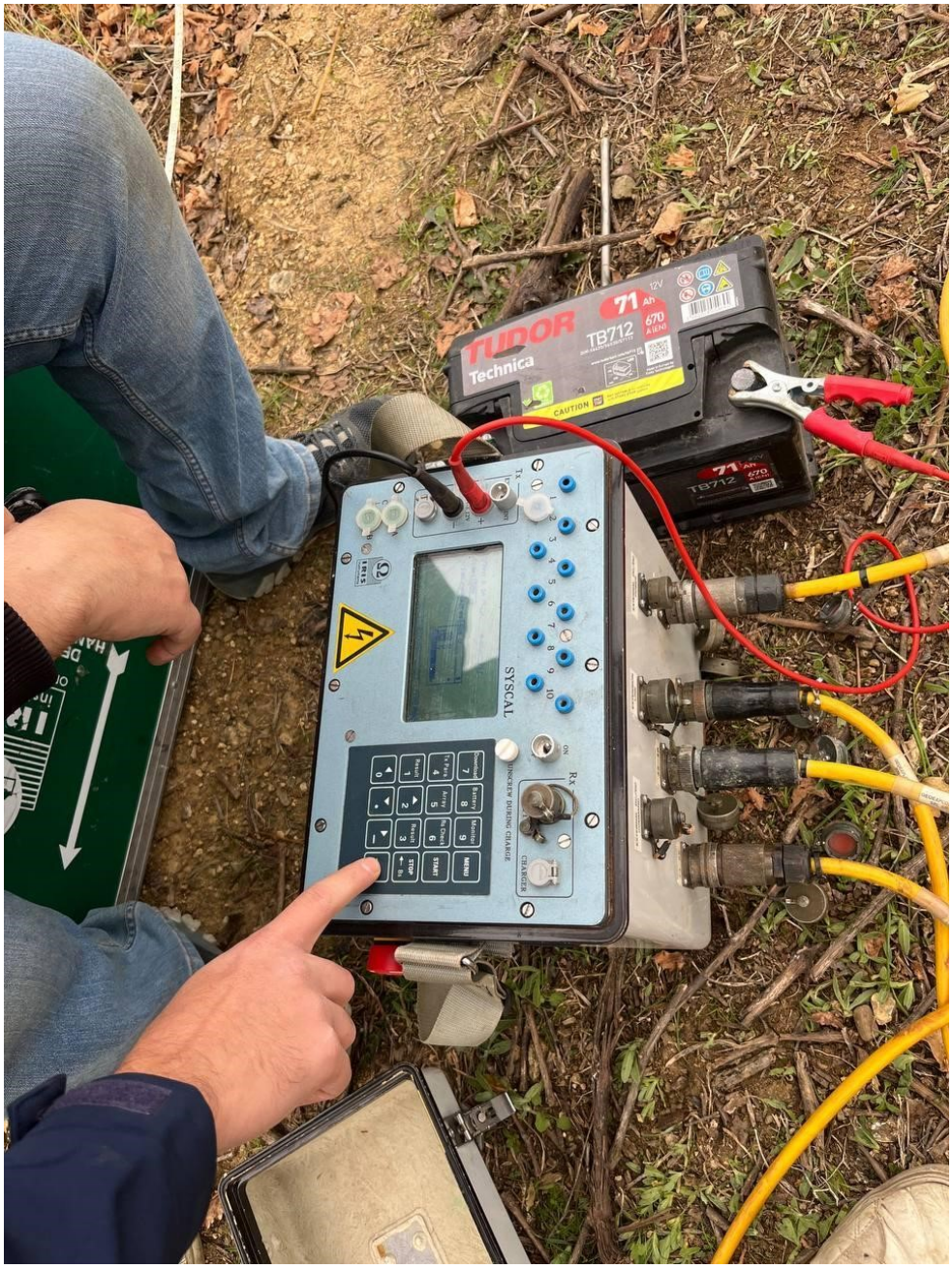

Figure 6.5. 3D ERT Data acquisition with syscal pro georesitivitimeter

Figure 6.6. Data acquisition with syscal pro georesitivitimeter

Before each acquisition, the contact resistances were regularly checked through the resistivimeter. An external 12V battery, connected to the Syscal, is used to generate the current for the acquisition. GPS coordinates were acquired (Figure6.7), and the measuring device was always placed at the center of each segment, between electrodes 48 and 49.

Figure 6.7. GPS data point measurement

6.2. OHM mapper

The resistivity measurements discussed in this thesis were performed with the Ohm Mapper. Unlike classic georesistivimeters, which use metal pegs (electrodes) or conductive fillings necessary to create electrical contact with the ground, the OhmMapper bases its operation on capacitively coupled electrodes, which induce current in the ground without the need for energization by contact. This occurs through the use of two or more 'antennas' (a transmitter

and one or more receivers) which are dragged by the operator via a system of cables connected to each other.

The advantages of this tool are multiple; first of all, it is possible to carry out rapid geoelectrical surveys (including tomography) in a short time. Furthermore, the measurements are not disturbed by contact resistance and therefore this instrument is excellent in high resistivity soils and/or on all surfaces where it would be difficult to implant the electrodes (asphalted or paved areas). The spatial resolution with which the terrain is investigated is linked only to the speed with which the operator walks and not to the overall number of electrodes: it is therefore possible to create high resolution resistivity sections for long distances. Finally, the acquisition speed and ease of maneuver make the OhmMapper ideal for creating resistivity plans and/or three-dimensional models.

The main limitations of the instrument are inherent in its very configuration: using induced current, in fact, it is not possible to energize the ground at great depths and the use of long coaxial 'antennas' limits its handling in confined environments. Finally, since the antennas must remain perfectly extended on the ground and in line with each other, the OhmMapper cannot be used on highly uneven terrain or characterized by morphological obstacles.

The receiver and transmitter are made up of dipolar coaxial cables (called 'antennas') having lengths multiples of 2.5 meters **(Figure 6.8)**; the distance that separates the receiver from the transmitter determines the investigation depth of the instrument. However, it must be remembered that the signal decreases with the cube of the distance between the antennas; for example, if you increase the separation between receiver and transmitter from 10 to 20 m, the signal is reduced by 1/8**(Table.6.1)**. The maximum investigation depth therefore depends on the maximum distance at which the receiver is able to measure a potential difference induced by the transmitter; in soils with high resistivity, it is possible to reach greater depths than in soils with higher conductivity. The depth of investigation can be varied by changing both the length of the cord separating the receiver and transmitter and the length of the 'antennas'.

CONFIGURAZIONE DIPOLO-DIPOLO

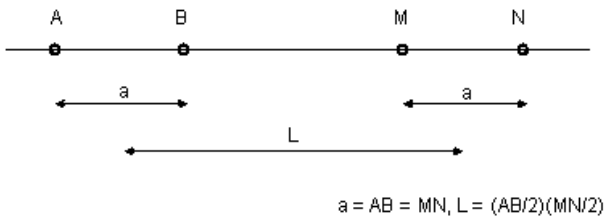

Table 6.1. depths reachable with the OhmMapper based on the length and distance between the antennas.

Antennas distance (BM)	Depth achieved with 2.5m antennas	Depth achieved with 5m antennas	Depth achieved with 10m antennas
0,625 m	0,50 m	0,82 m	/
1,25 m	0,68 m	1,01 m	1,64 m
2,5 m	1,04 m	1,37 m	2,01 m
5 m	1,74 m	2,09 m	2,74 m
7,5 m	2,40 m	2,79 m	3,46 m
10 m	3,05 m	3,47 m	4,17 m
12,5 m	3,69 m	4,15 m	4,88 m
15 m	4,31 m	4,81 m	5,57 m
17,5 m	4,94 m	5,46 m	6,26 m
20 m	5,57 m	6,10 m	6,95 m

The data were collected in the same 15mx15m square profile, but this time perpendicular to the ERT measurements in 6 parallel lines **(Figure 6.2)**. In this type of measurement, we first set two points in each line as the initial and final points with GPS, and in the next step, we started the measurement with a 10 meters non-conductive rope as the distance between the antennas **(Figure 6.10)**. In the next step, the measurement was done with a 5-meter rope and finally, with a 1.25-meter rope **(Figure 6.11)**. This process was done in the same way in all lines **(Figure 6.12, 6.13)**.

Figure 6.10. non-conductive rope in ohm mapper measurement.

Figure 6.11. ohm mapper measurement with 1.25m non-conductive rope.

Figure 6.12. OHM mapper Data measurement

Figure 6.13. OHM mapper Data measurement

7. Processing and Inversion

7.1. Processing

7.1.1. 3D ERT

ERT measurements are affected by errors that need to be properly considered as they could influence the inversion process. Typically, these errors arise as a consequence of poor contact between electrodes and the ground, low current injection or other random external effects. Therefore, an appropriate error assessment is recommended to avoid annoying effects on the inversion procedure, as artifacts or heavy smoothing. All the gathered data were analyzed, processed with ProsysII and visualized with ERT Lab software.

Due to the ERT measuring method, first outliers were defined as those with collected potential readings below 1 mV. The same applied for negative R measured values, clearly related to poor contact between the electrodes and the ground.

All 5049 measurements obtained were apparent resistivity data. These were imported into ProsysII software. Subsequently, anomalies were noted in some data points where the apparent resistivity was recorded as below zero as misfit data. By applying a filter, all misfit data were removed, resulting in a dataset of 4900 apparent resistivity measurements. The apparent resistivity values now ranged mostly from 10Ω to approximately 100Ω **(Figure 7.1)** as illustrated as a 3DPseudosection **(Figure 7.2)**.

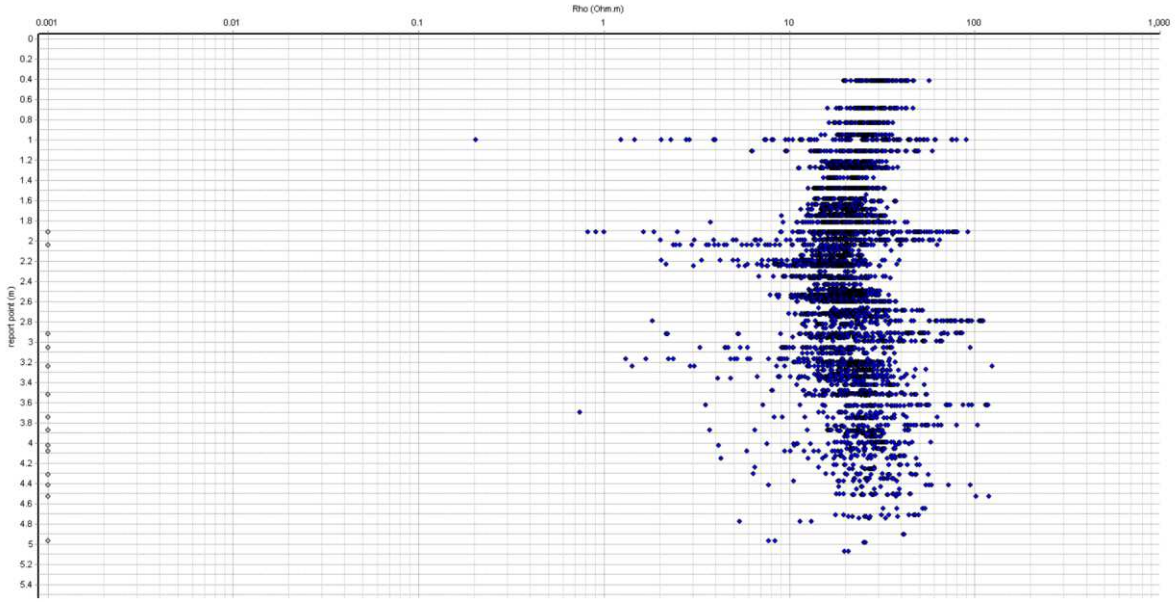

Figure 7.1. The apparent resistivity values after exterminating bad data point with prosysII

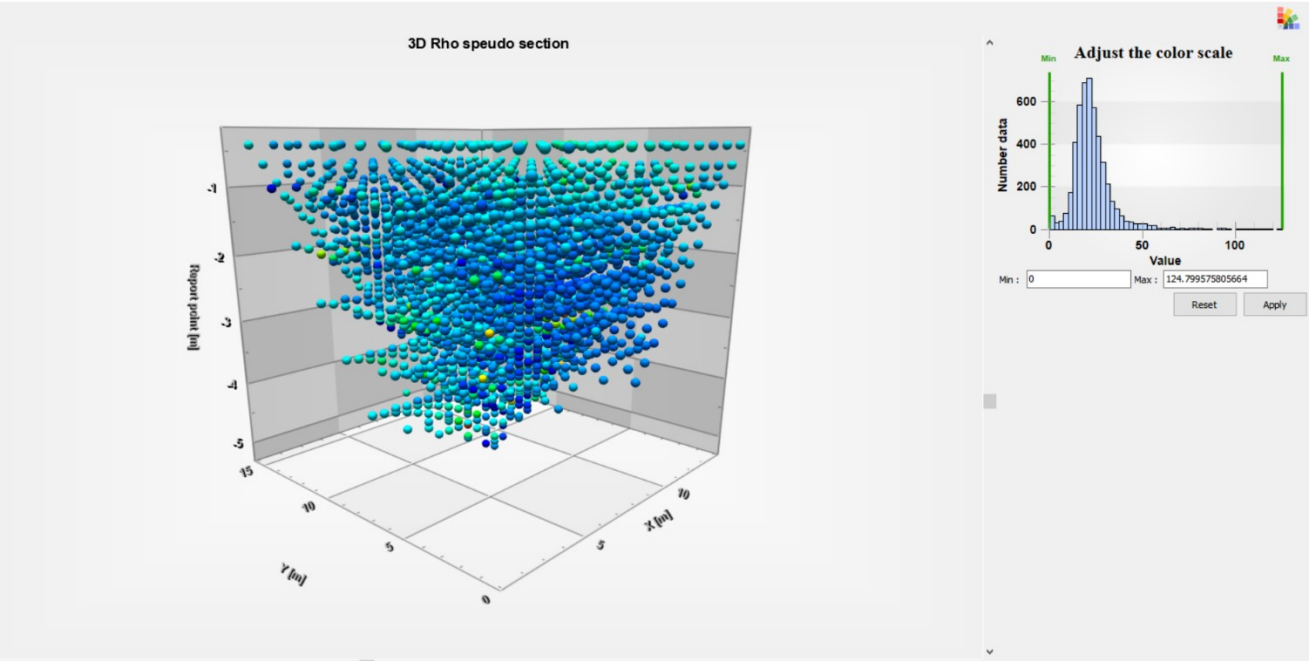

Figure 7.2. 3D Pseudosection after the filtering process with ProsysII software

Following the processing of all data using ProsysII software, the next step involves generating a 3D pseudosection utilizing ERT Lab software, wherein the exact positions of all 96 electrodes are

indicated based on GPS data points **(Figure 7.3)**. According to 3D pseudosection, the maximum depth of measurement is around 10m. Also, most apparent resistivity data ranged are lower than 30Ω (blue data point).

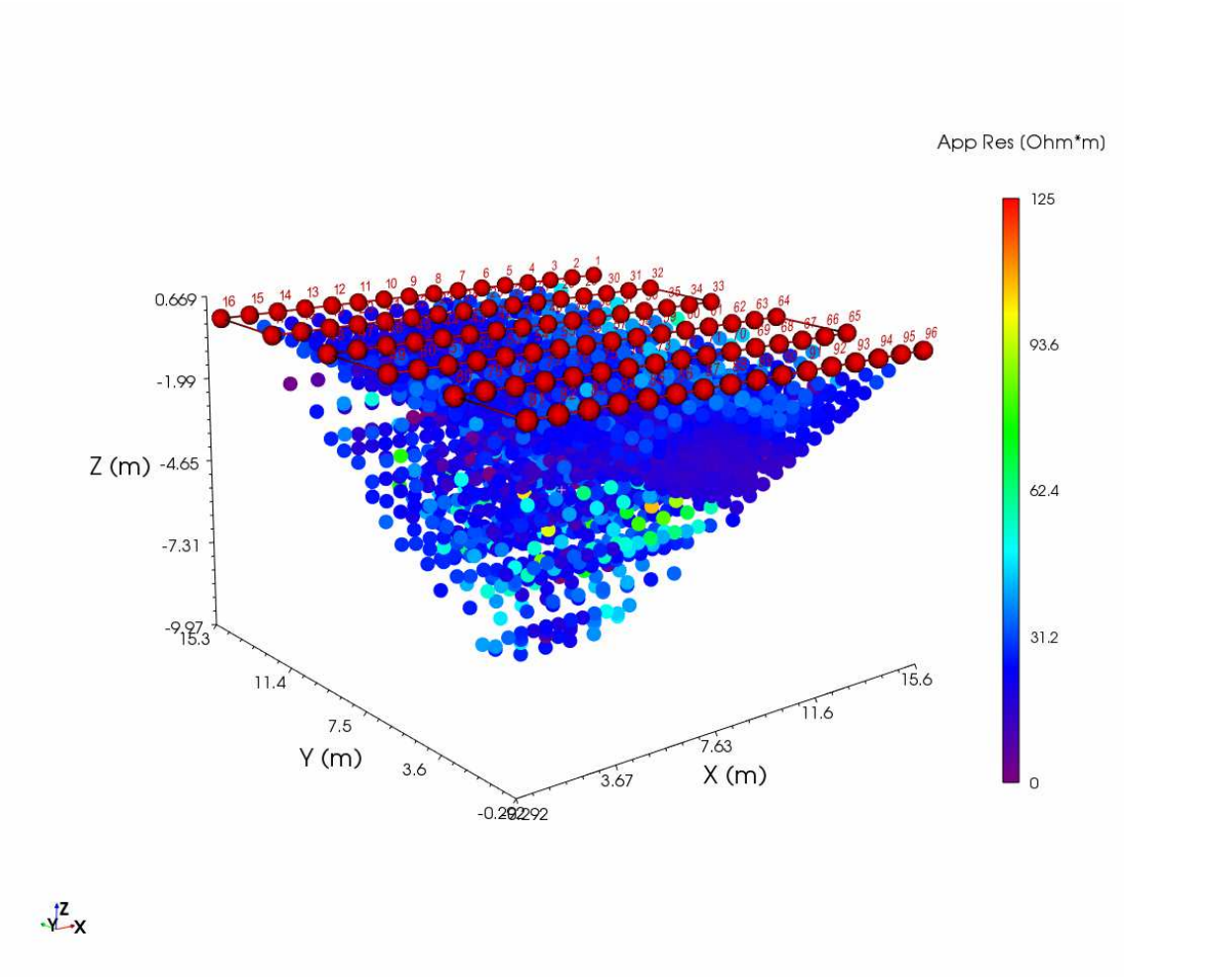

Figure 7.3. 3D Pseudosection after the filtering process with all electrodes position and their paths with ERT Lab software

7.1.2. OHM mapper

Following an exposition of the theoretical principles governing the operation of field instruments, as well as a delineation of the data collection procedures utilizing the OhmMapper and GPS, this chapter aims to elucidate the geophysical data processing methods facilitated by two specialized

software programs: MagMap2000 (Geometrics) and Res2Dinv. These applications enabled the derivation of resistivity tomography from the field-measured parameters. The function of the MagMap2000 software is mainly to import the data, stored on the console in Binary Data (.bin) format, into the PC and convert it to ASCII format which display geometry survey such as length of profile, the direction of travel, and the spacing of marks **(Figure 7.4)**. It is also possible to correct the information collected by making corrections on the arrangement of the marks and on the geometry of the various paths taken with the OhmMapper tool during the data collection **(Figure 7.5)**

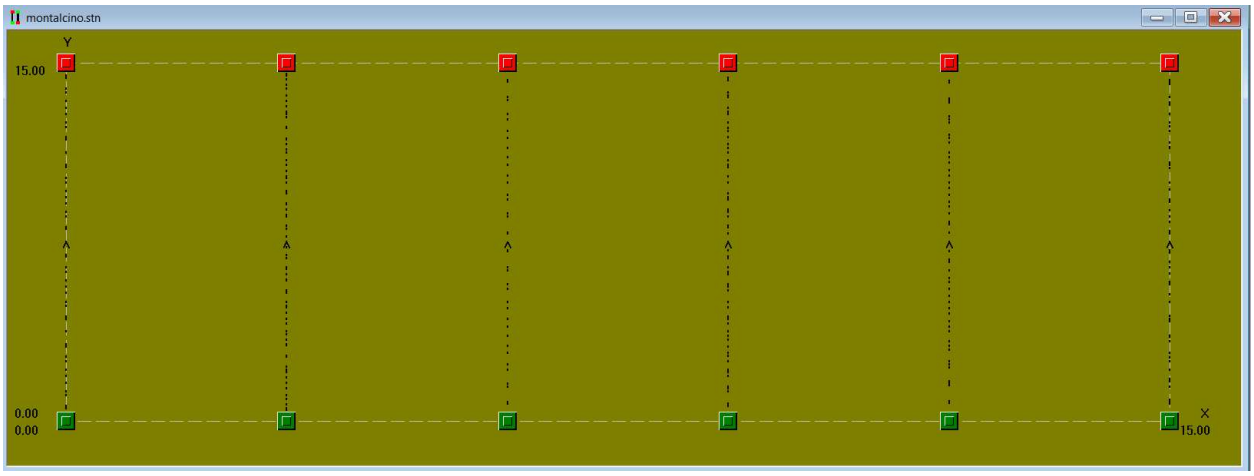

Figure 7.4. survey geometry displayed on MagMap2000; the length of the profile, the direction of travel and the spacing of the marks used are represented.

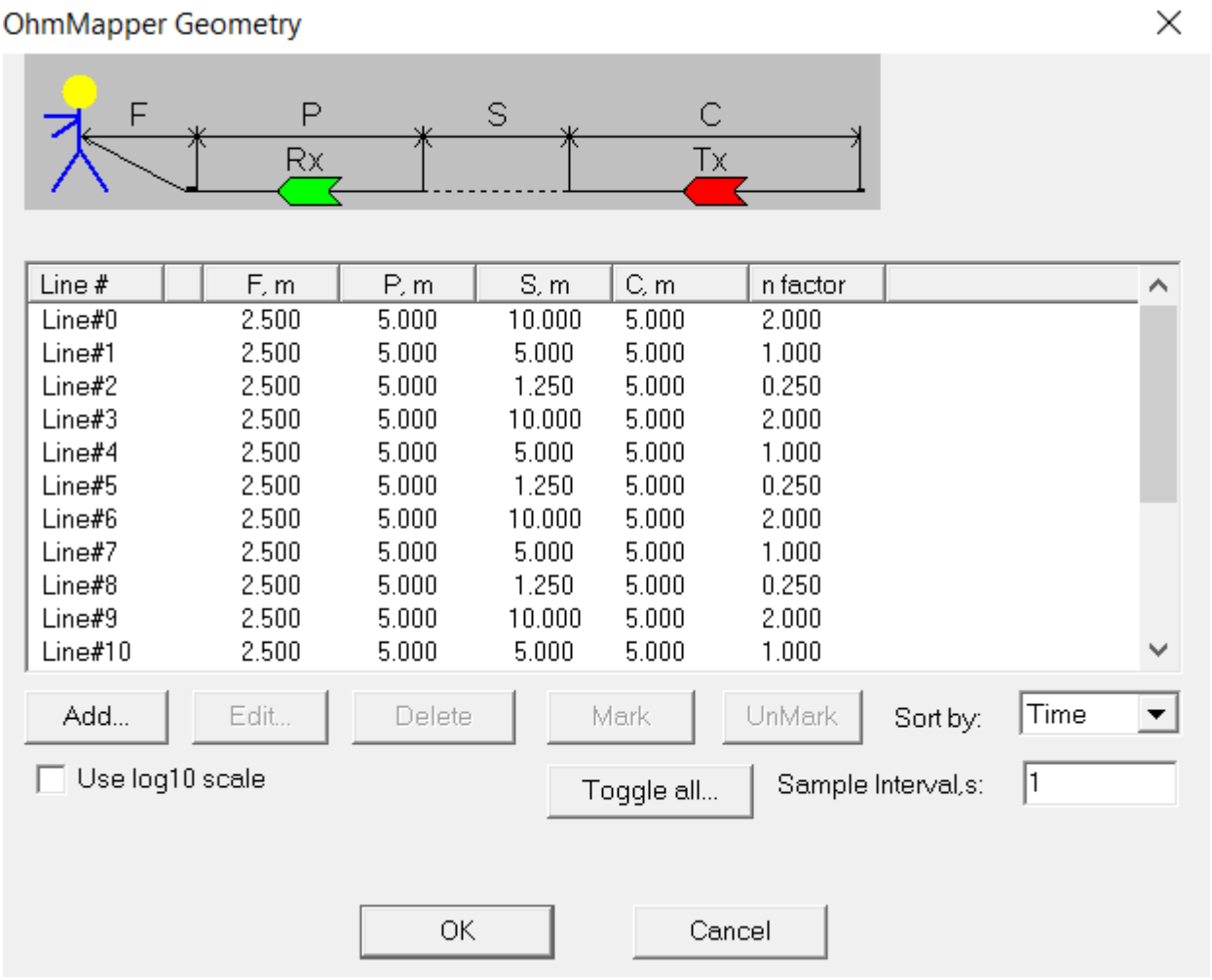

Figure 7.5. Window that opens by selecting the "Plot resistivity map" command: the geometry of the instrument configuration for the various profiles is schematized. The n factor is obtained from the ratio between the distance in meters that separates the receiver from the transmitter and the length of the antennas in meters; as the n factor varies, the depth of investigation also varies

According to MagMap, the potential difference measurements (ΔV) can be displayed in a graph as a function of the acquisition instant using the "Plot OhmMapper readings" command **(Figure 7.6)**; this data visualization allows you to distinguish the signal from the noise and possibly remove spurious signals with filters such as, for example, despike and smoothing. Binary files can be transformed into ASCII (.stn) format and exported as WinSurf Data (.dat) files for use in the next inversion step.

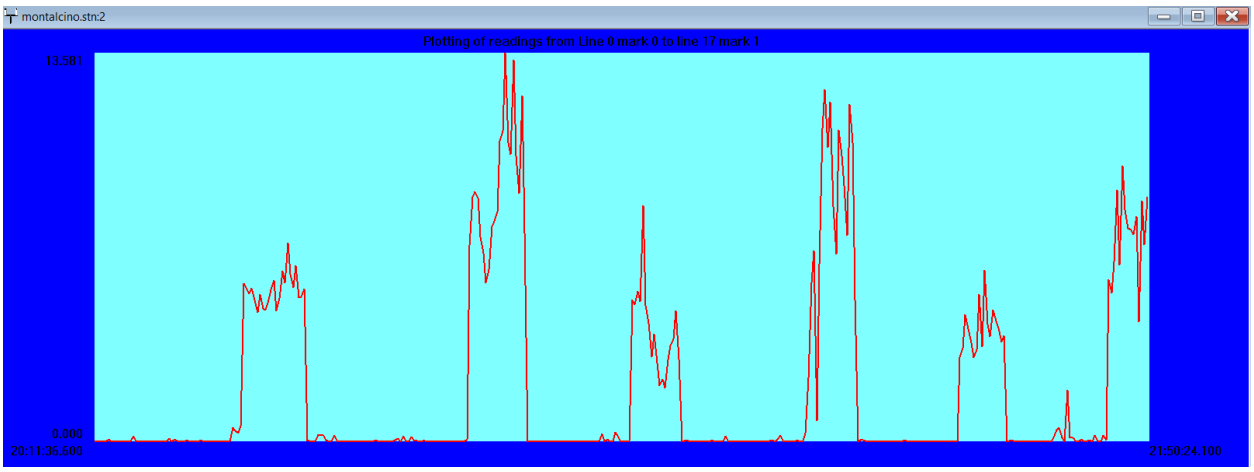

Figure 7.6. graph representing the ΔV values measured as a function of time; sudden spikes often represent signal disturbances (noise).

After using some filters such as despike and smoothing, it's time to display 2D Pseudosection for each line by click on draw pseudosection along Y axis **(Figure 7.7,7.8,7.9,7.10,7.11,7.12)**.

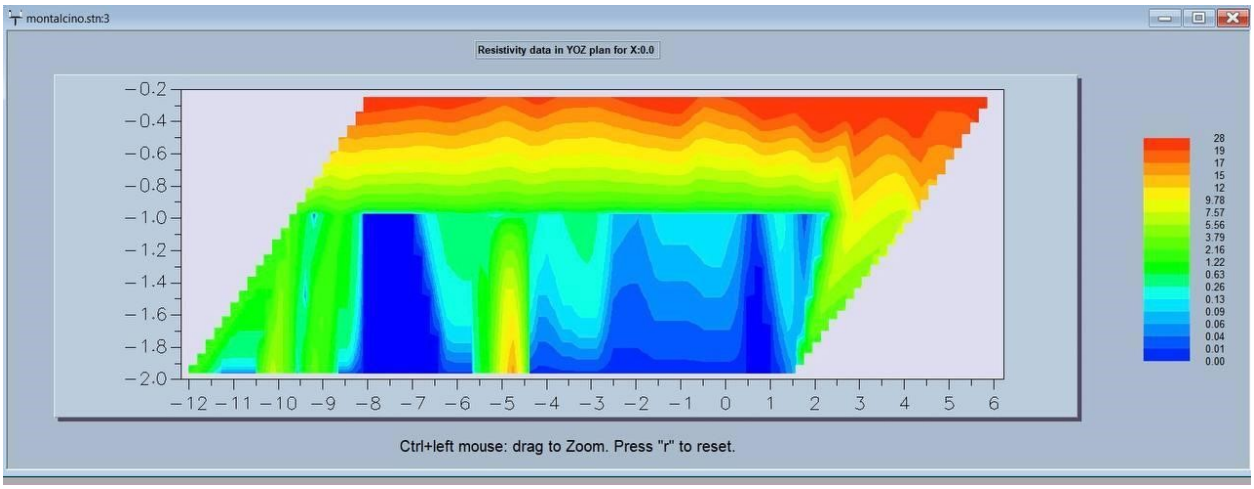

Figure 7.7. 2D pseudosection for line number 1 with magmap

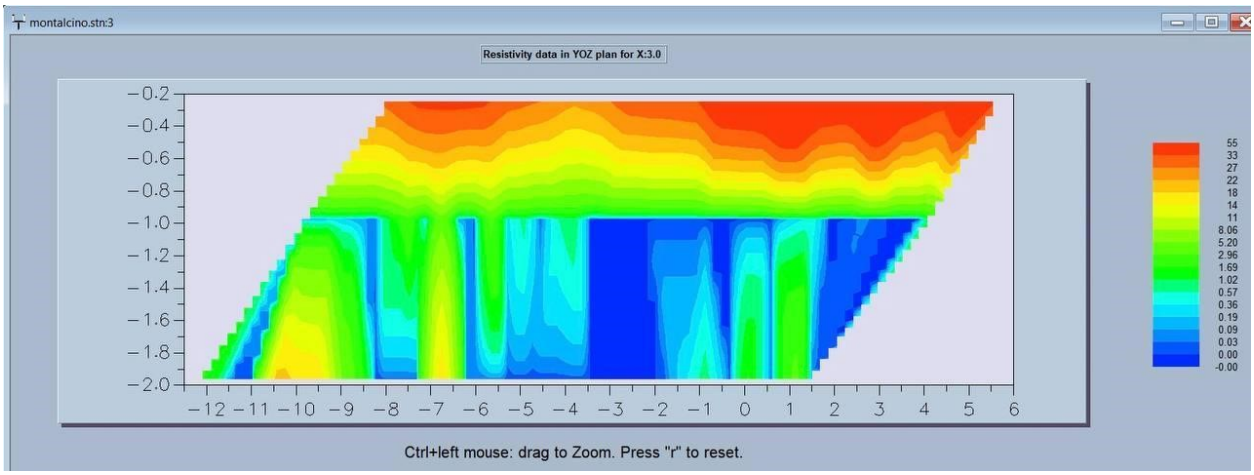

Figure 7.8. 2D pseudosection for line number 2 with magmap

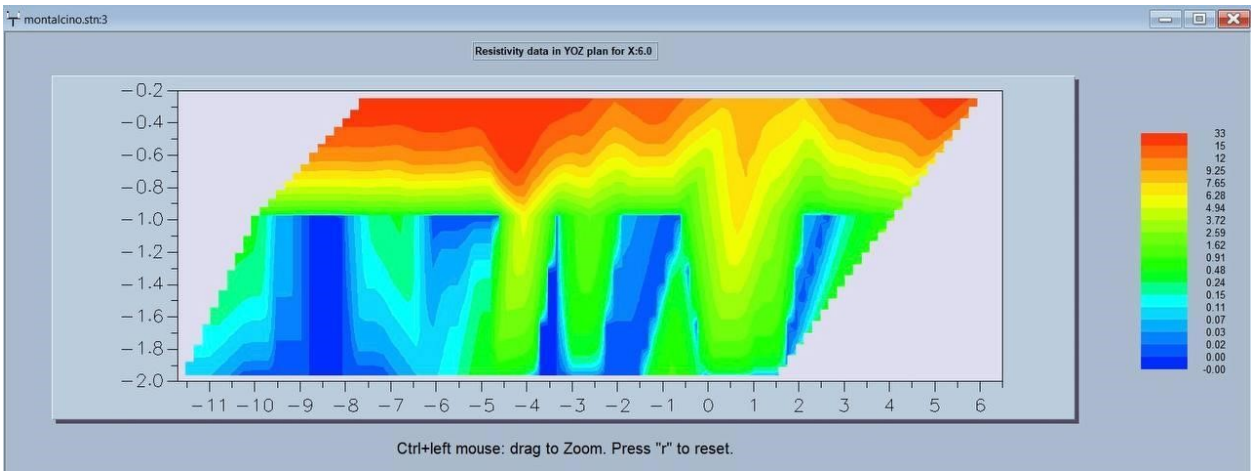

Figure 7.9. 2D pseudosection for line number 3 with magmap

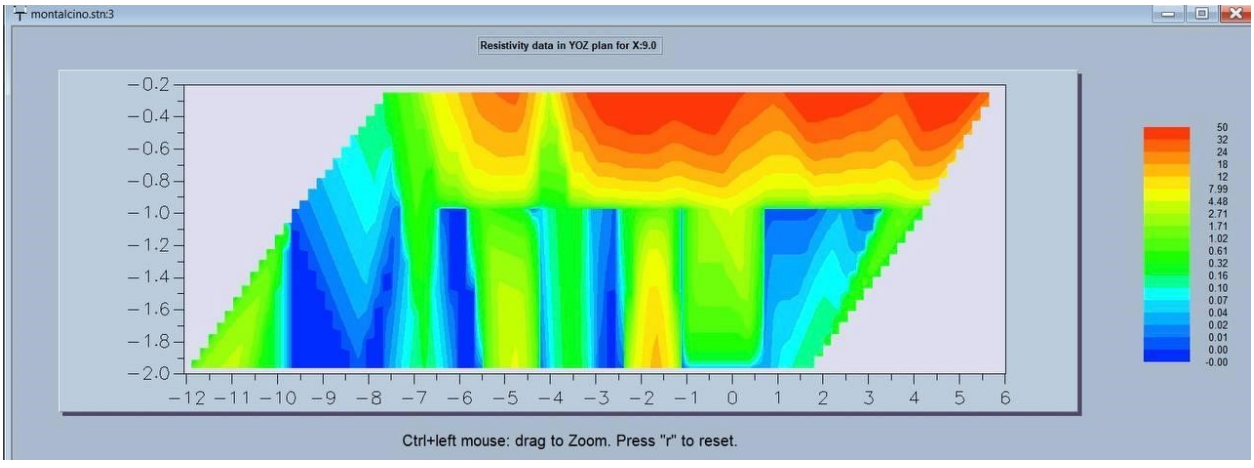

Figure 7.10. 2D pseudosection for line number 4 with magmap

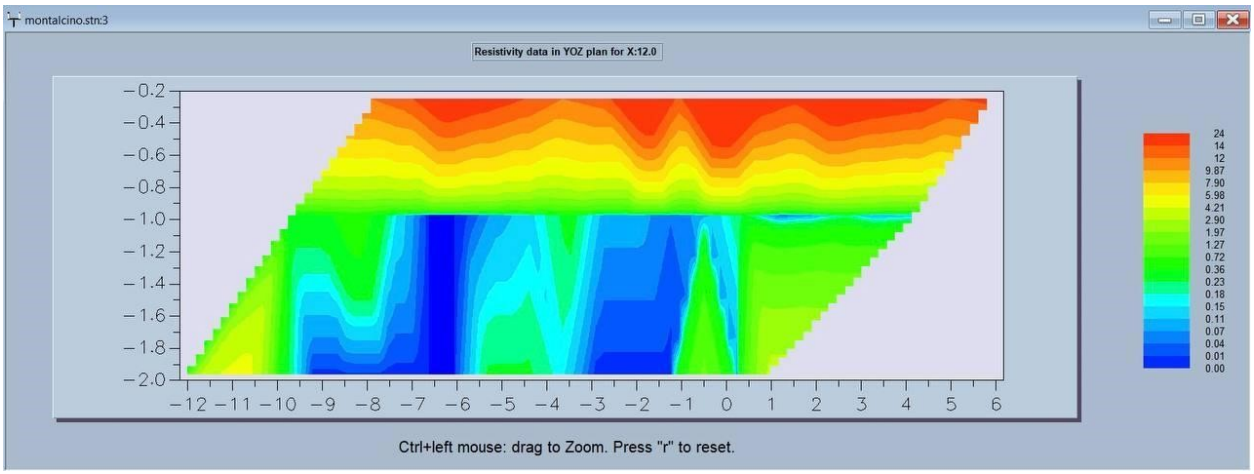

Figure 7.11. 2D pseudosection for line number 5 with magmap

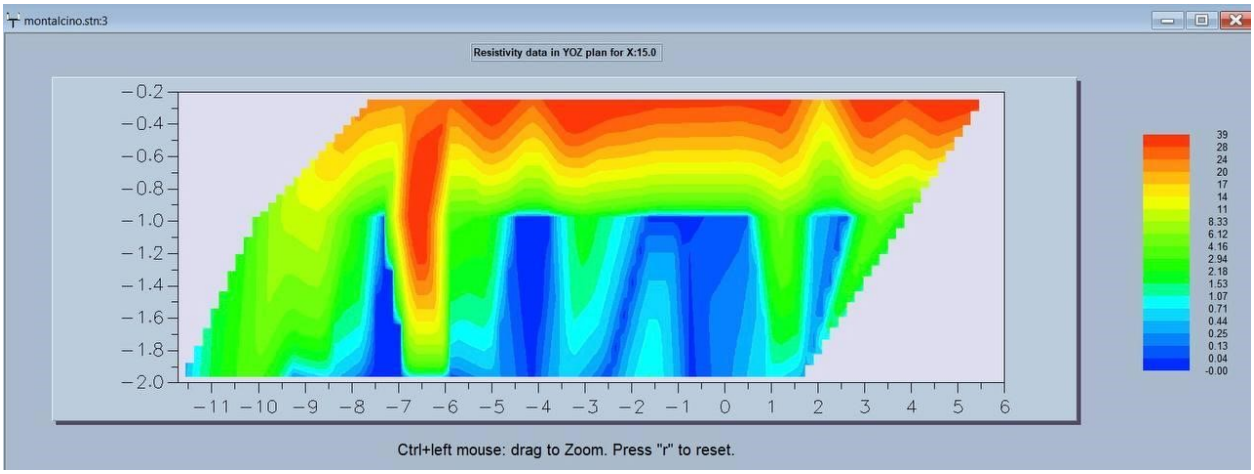

Figure 7.12. 2D pseudosection for line number 6 with magmap

7.2. Inversion Modeling

7.2.1. 3D ERT

The main purpose of the ERT method is to acquire the distribution of electrical properties about the interior of a domain based on a set of measurements conducted on its surface. The investigated system is mathematically determined by a discrete model, obtained by computing theoretical responses from an assumed distribution of the electrical properties.

This electrical forward problem, to be solved, requires the employment of numerical methods (i.e. finite element or finite difference), which are based on a representation of the domain realized through a grid or a mesh, made of several nodes and elements. Hence, the solution representing the potential field is provided at each node.

To compute the real resistivity distribution that explains the dataset made of our electrical measurements, however, the "inverse problem" needs to be solved. Given some measured quantities collected on the surface, we use a theoretical relationship to derive the values of the set parameters of a model that reproduces the given field observations. This approach is based on iteratively minimizing an objective function comprising both data misfit (measured and modeled) and a penalty term which considers deviations from the desired model.

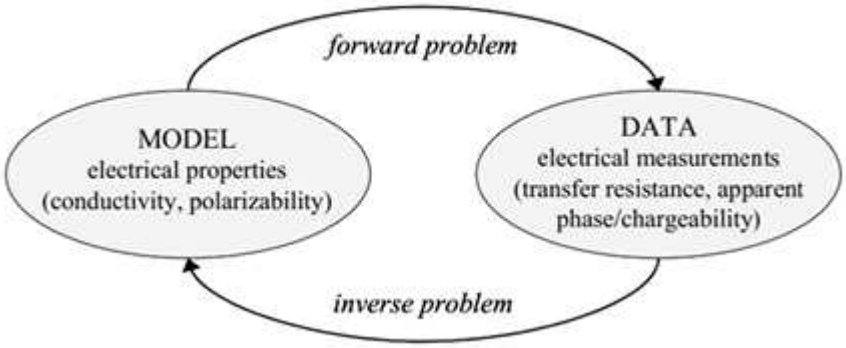

Figure 7.13. Definition of electrical forward and inverse problem.

In this study, 3D ERT data were inverted with RES3DINV software. RES3DINV software uses an algorithm based on least squares which allows to determine a three-dimensional resistivity model of the portion of the subsoil investigated: the potential difference measured by the receiver depends not only on the resistivity values of the materials but also on the geometry of these materials. The inversion process has the prerogative of identifying a model in accordance with the measurements collected which adequately represents both the resistivity values obtained but also their distribution in space. The RMS (Root Means Square) expressed as a

percentage indicates how well the apparent resistivity measurements agree with the calculated model. Once the data undergo processing in ProsysII software, the initial step involves converting them into RES3DINV format. Subsequently, upon importing the data into the software, one must navigate to the inversion settings tab to select the desired number of iterations, setting them to four times to minimize RMS error. Finally, after adjusting all the necessary parameters in the settings tab, it is time to execute the inversion process to visualize the inversion model **(Figure 7.14)**.

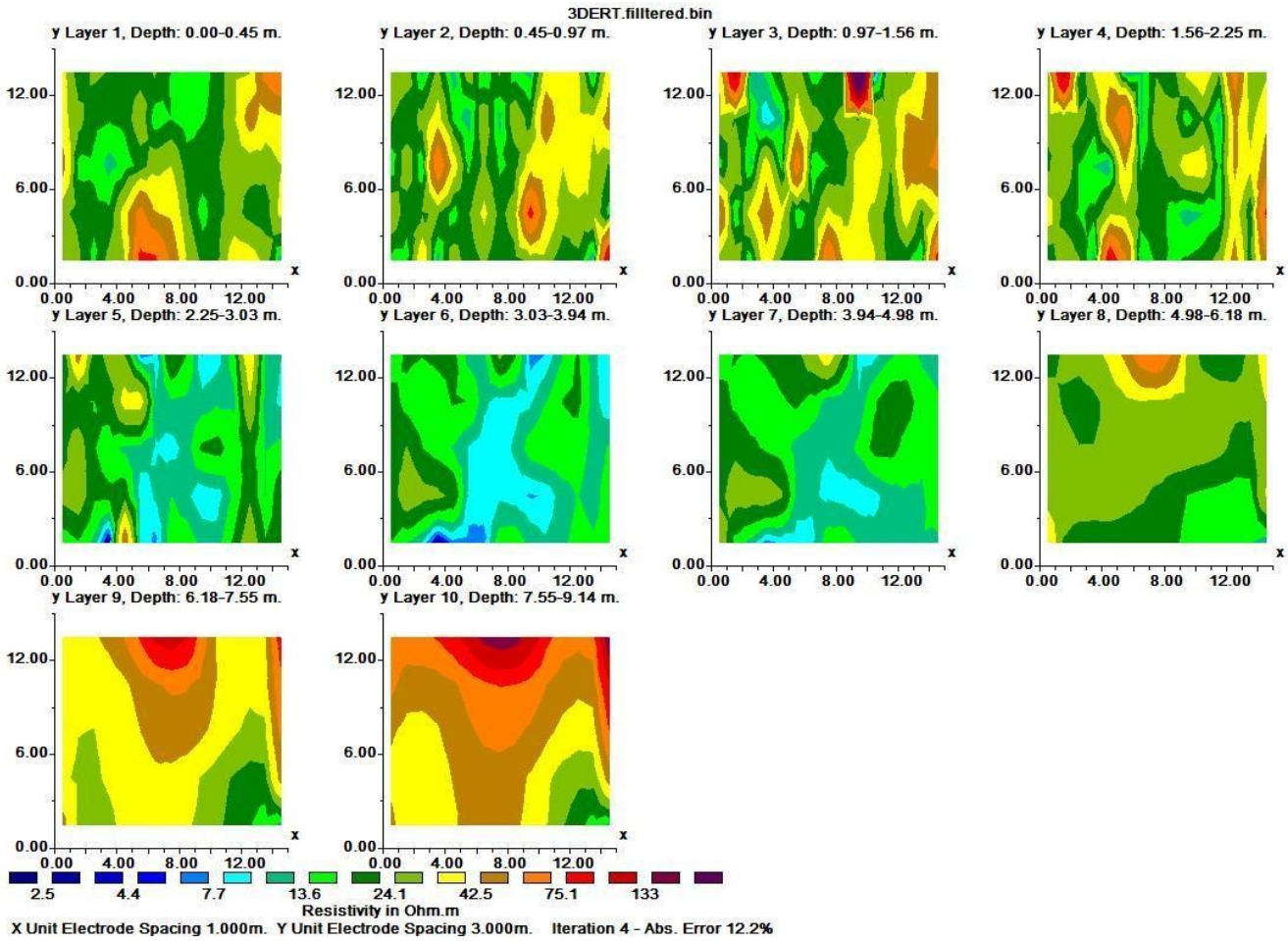

Figure 7.14.3D inversion model, Horizontal section, slice XY

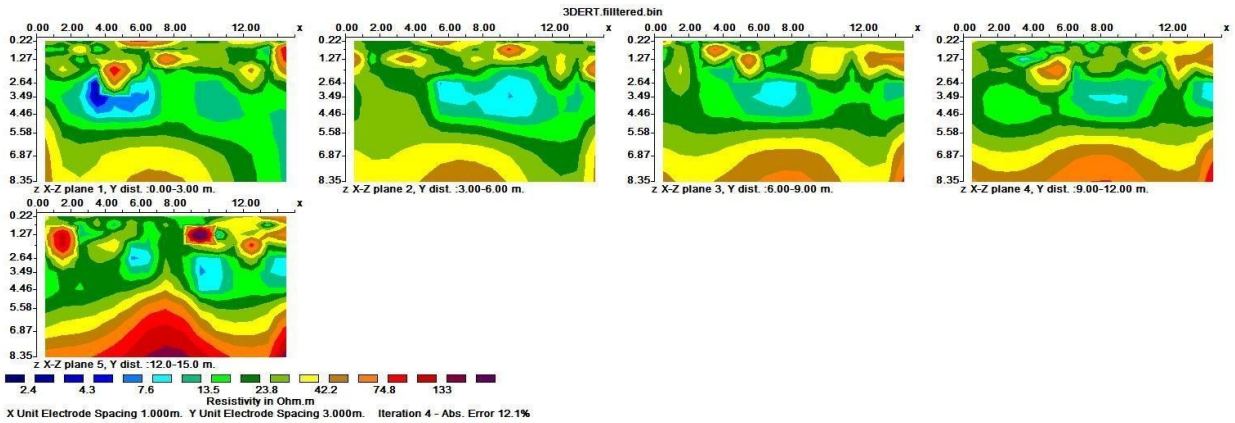

Figure 7.15. 3D inversion model, vertical section, slice xz

As RES3DINV is a proprietary software, accessing the 3D model visualization requires a valid license, which may not always be feasible. To address this limitation, we employed RESIPy software to resolve the issue. Upon importing the data into the software, given that the data have already undergone processing, we proceed directly to the inversion settings. Within this tab, it's important to employ normal regularization and adjust the number of iterations to four. It's recommended to estimate a_wgt and b_wgt based on error checks in the field data, preferably derived from reciprocal measurements rather than repeatability measures. Typically, for surface data, a_wgt is approximately zero ohms, while b_wgt is around 0.01, roughly corresponding to a 1% error. Once all essential inversion parameters are adjusted, the 3D inversion model can be visualized **(Figure 7.16),** and display horizontal section in surface **(Figure 7.17)**, at depth of 1.5m**(Figure 7.18)**, and depth of 2.5m**(Figure 7.19)** and vertical section when Y=0 **(Figure 7.20)**.

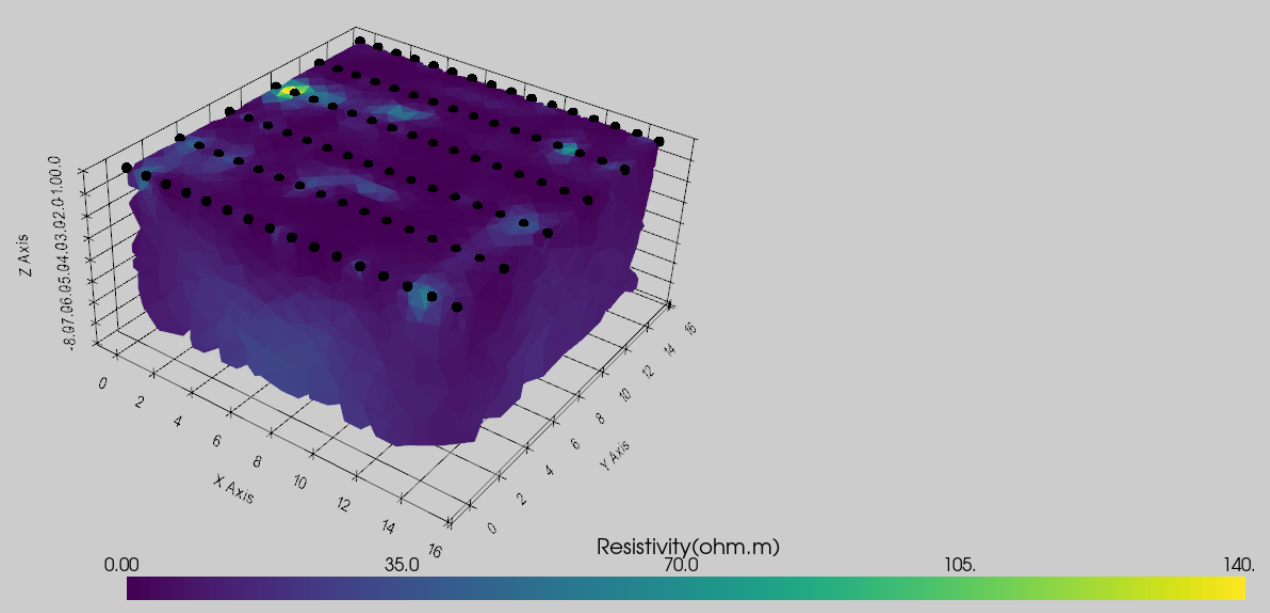

Figure 7.16. Visualize 3D ERT inversion model

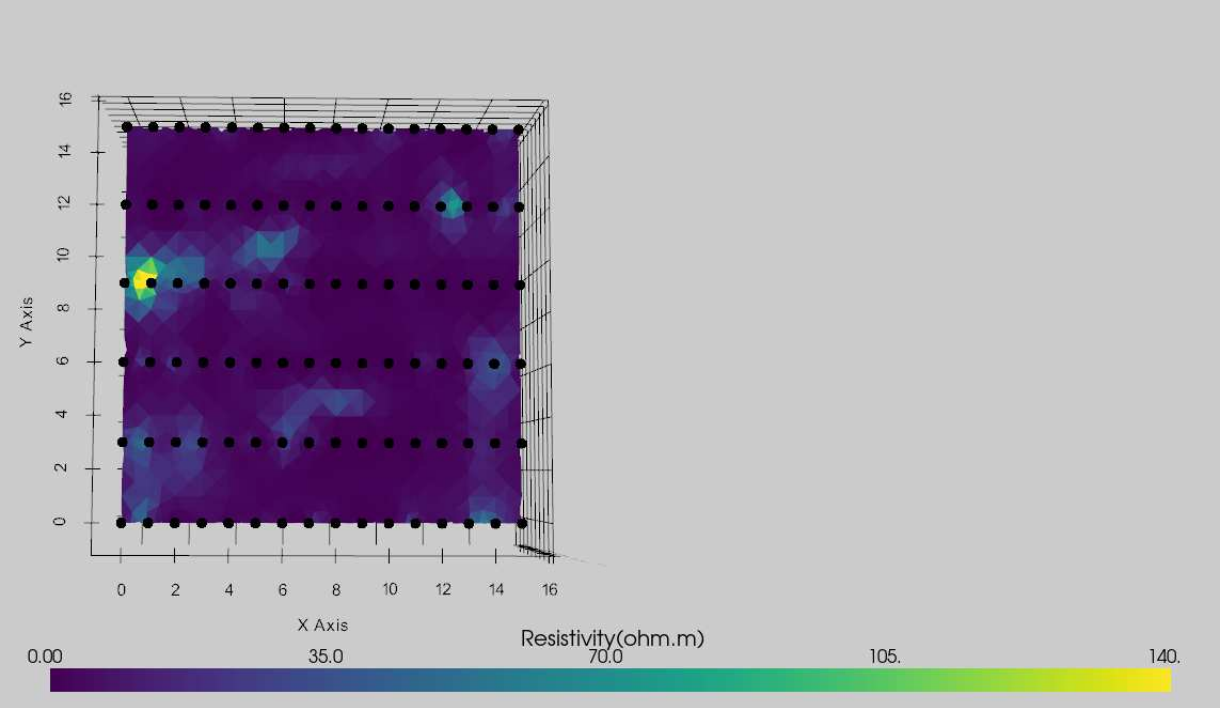

Figure 7.17. 3D inversion model, Horizontal section, slice xy, Z=0

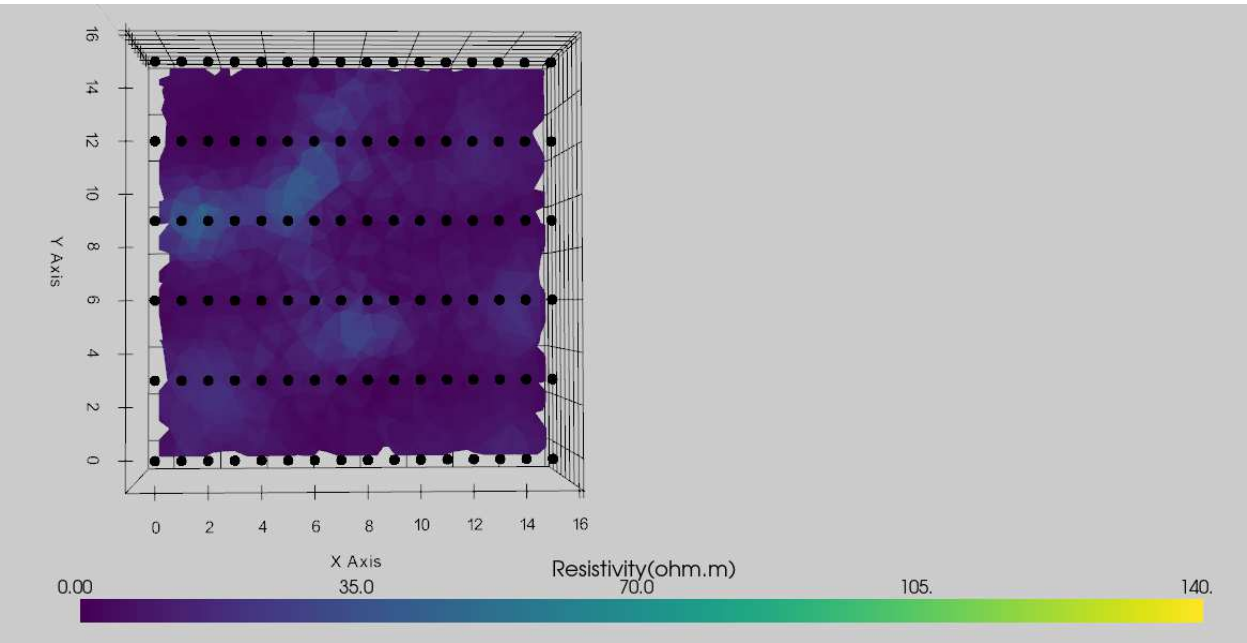

Figure 7.18. 3D inversion model, Horizontal section, slice xy, Z=1.5

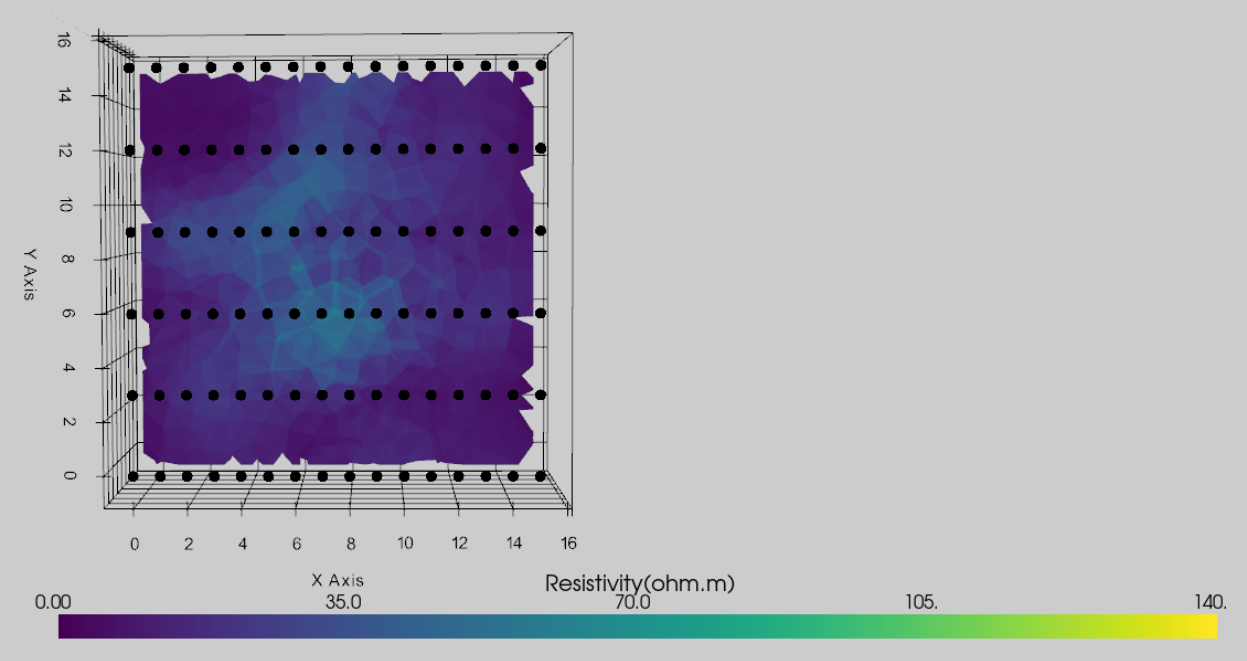

Figure 7.19. 3D inversion model, Horizontal section, slice xy, Z=2.5

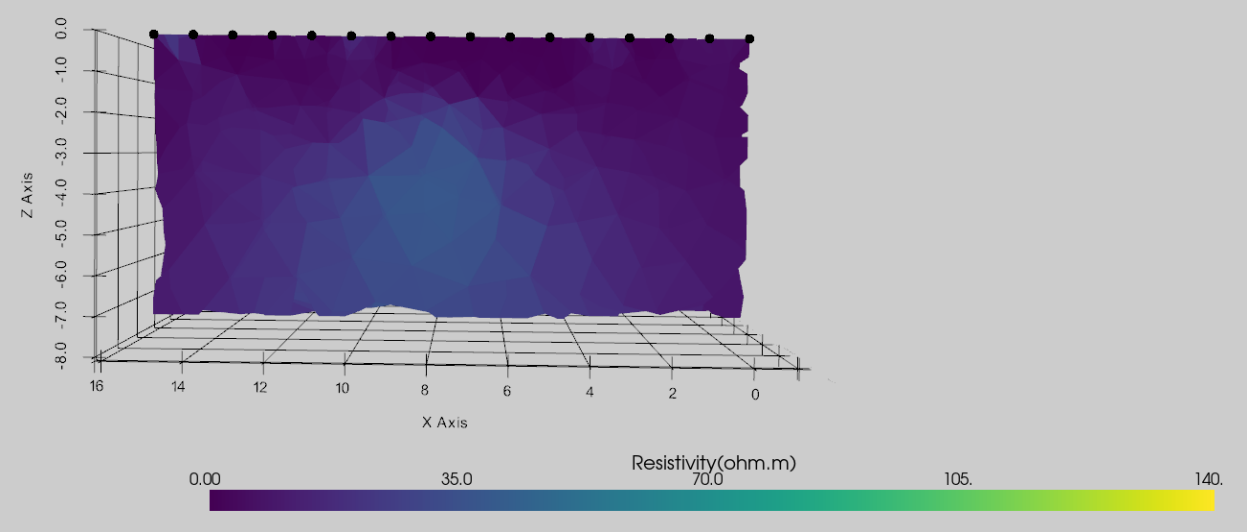

Figure 7.20. 3D inversion model, vertical section, slice xz, Y=0

7.2.2. OHM mapper

The outputs obtained from the MagMap2000 software were processed and inverted with the RES2DINV inversion program to obtain resistivity tomography in each of 6 lines **(Figure 7.21,7.22,7.23,7.24,7.25,7.26)**. The RES2DINV software uses an algorithm based on least squares which allows to determine a two-dimensional resistivity model of the portion of the subsoil investigated: the potential difference measured by the receiver depends not only on the resistivity values of the materials but also on the geometry of these materials. The inversion process has the prerogative of identifying a model in accordance with the measurements collected which adequately represents both the resistivity values obtained but also their distribution in space. The RMS (Root Means Square) expressed as a percentage indicates how well the apparent resistivity measurements agree with the calculated model.

Subsequently, upon importing the data into the software, one must navigate to the inversion settings tab to select the desired number of iterations, setting them to four times to minimize RMS error. Finally, after adjusting all the necessary parameters in the settings tab, it is time to execute the inversion process to visualize the inversion model.

In this chapter the 6 tomographies obtained from the surveys are processed and inverted with the RES2DINV. The inversion process has always highlighted low RMS values and has led to tomographies whose color scale has been made homogeneous to facilitate comparison both with the expected resistivity values and between the different tomographies.

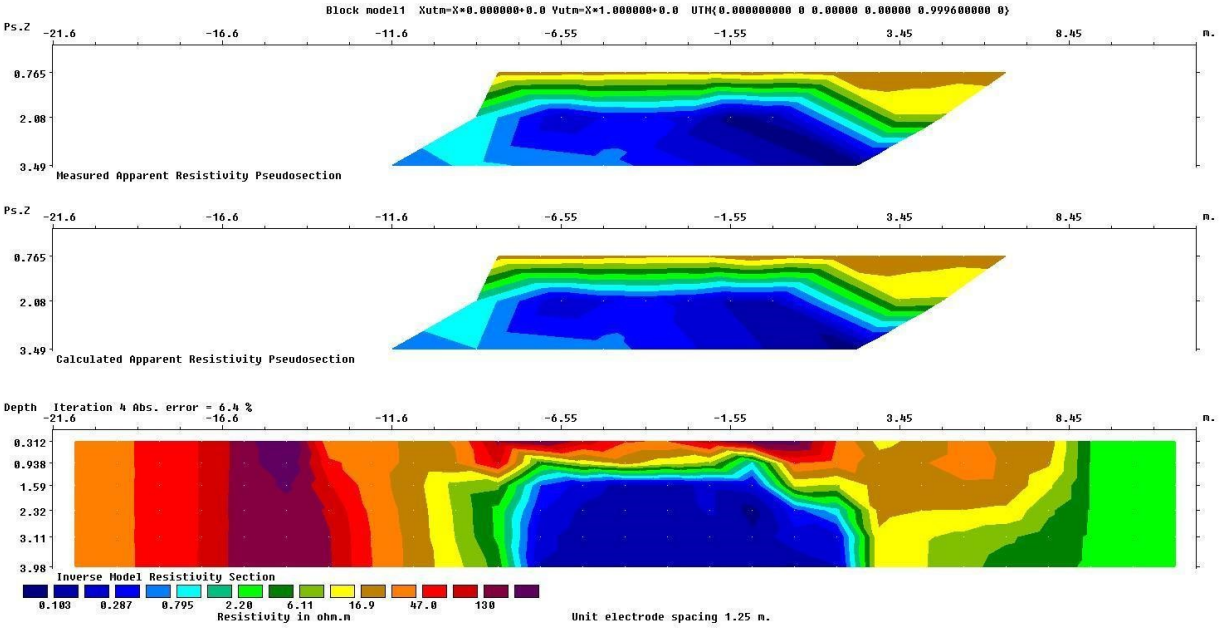

Figure 7.21. 2D inversion model for line number 1

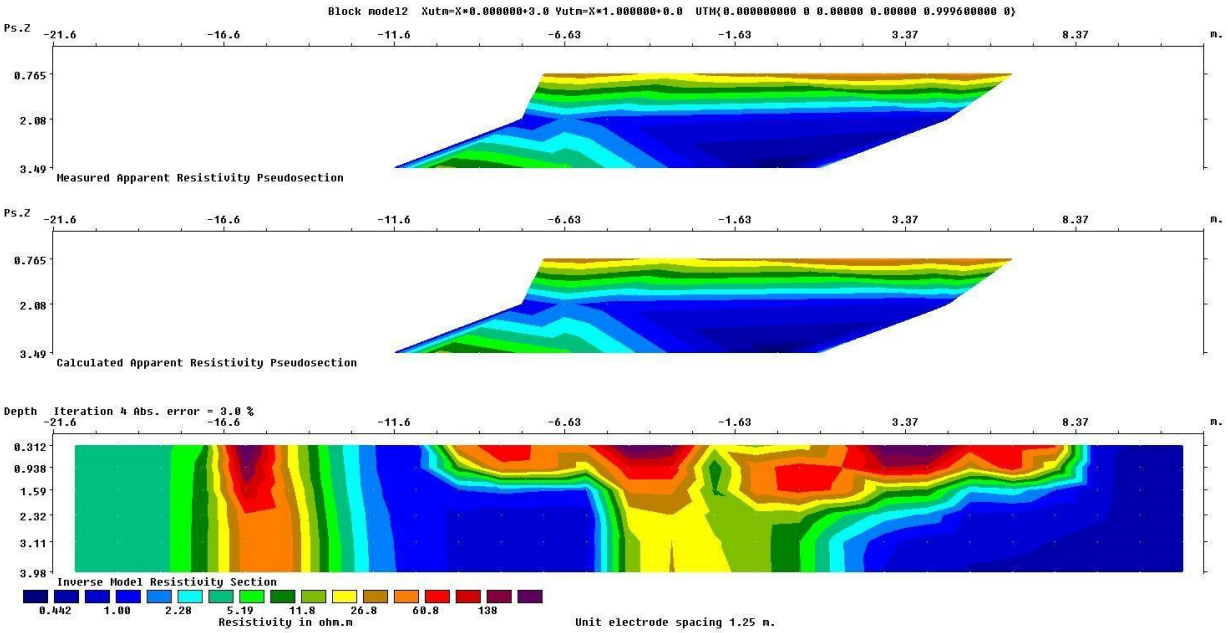

Figure 7.22. 2D inversion model for line number 2

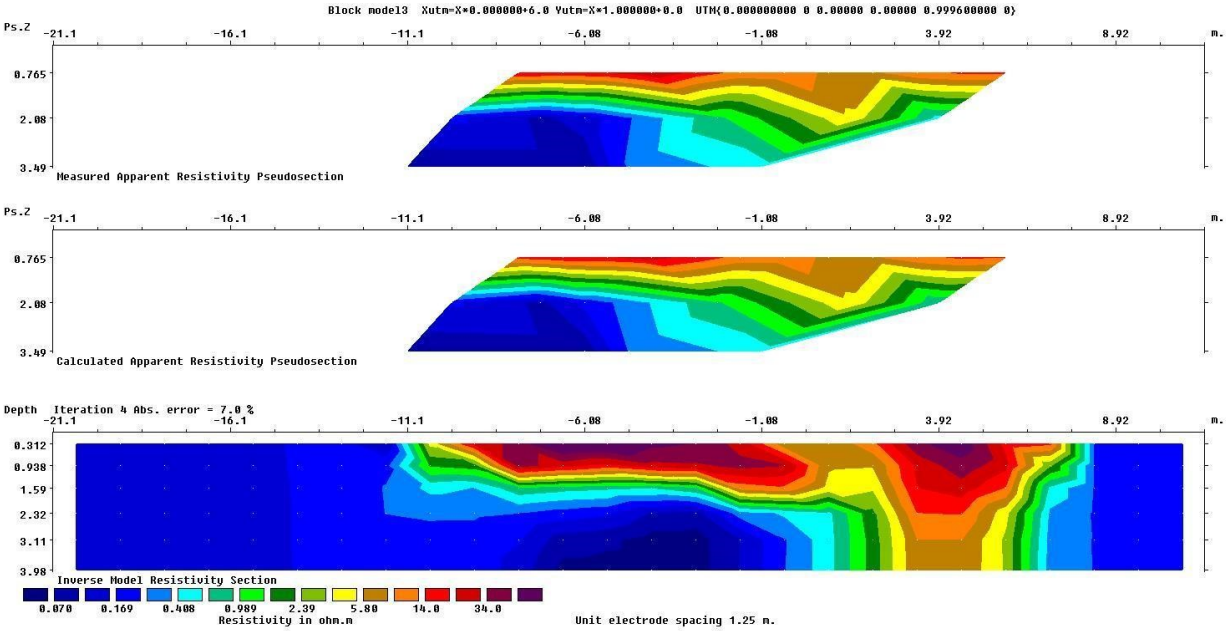

Figure 7.23. 2D inversion model for line number 3

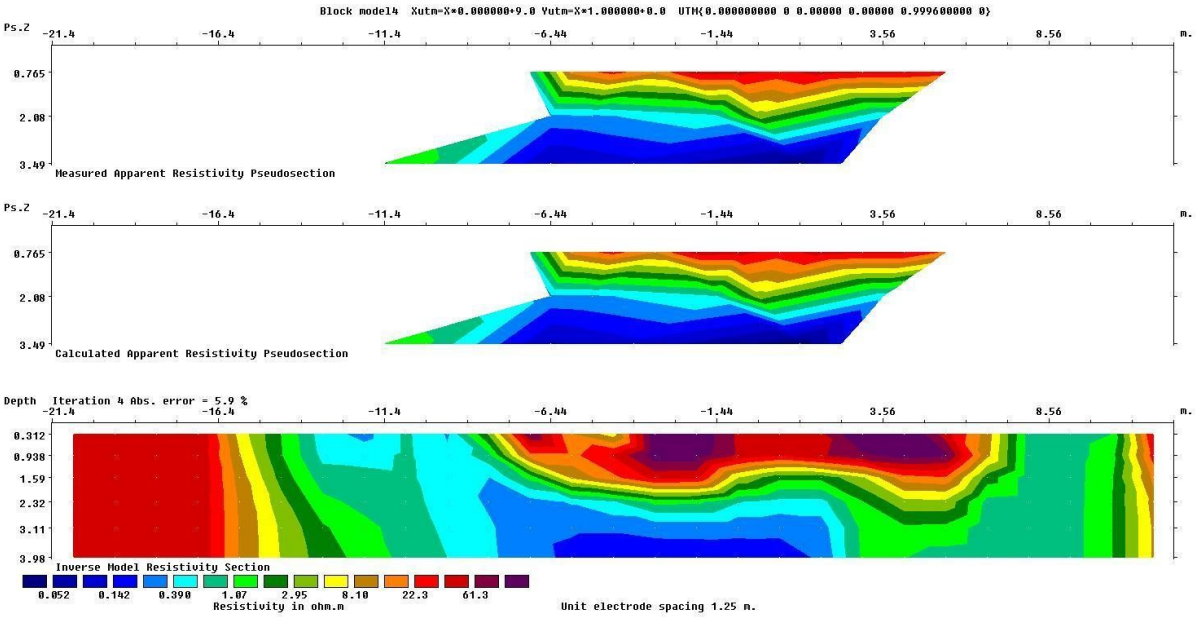

Figure 7.24. 2D inversion model for line number 4

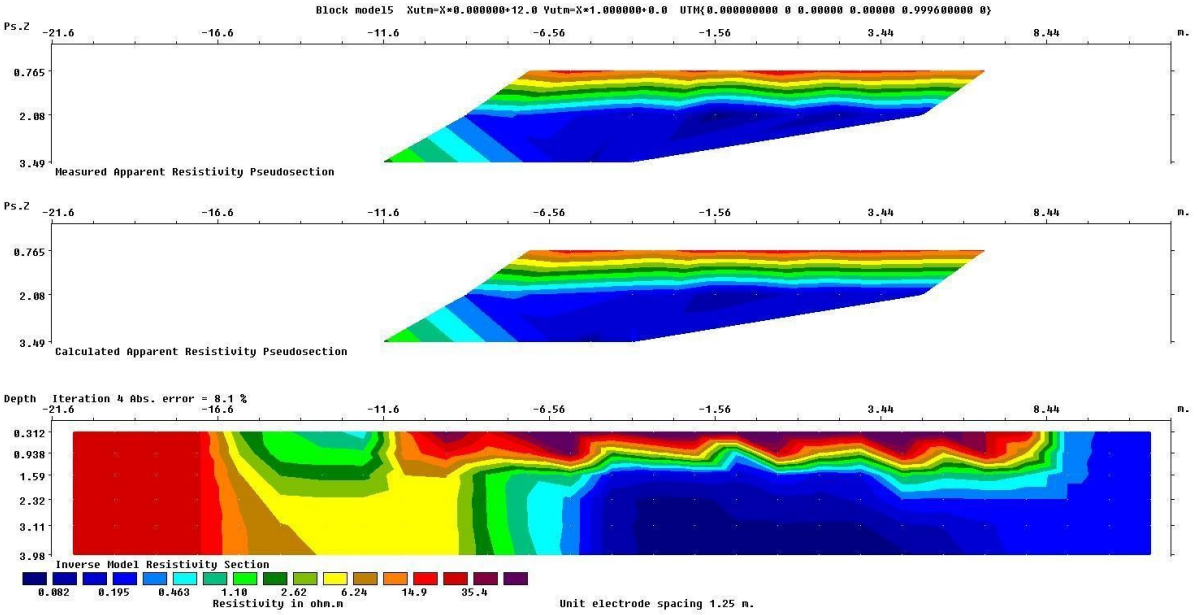

Figure 7.25. 2D inversion model for line number 5

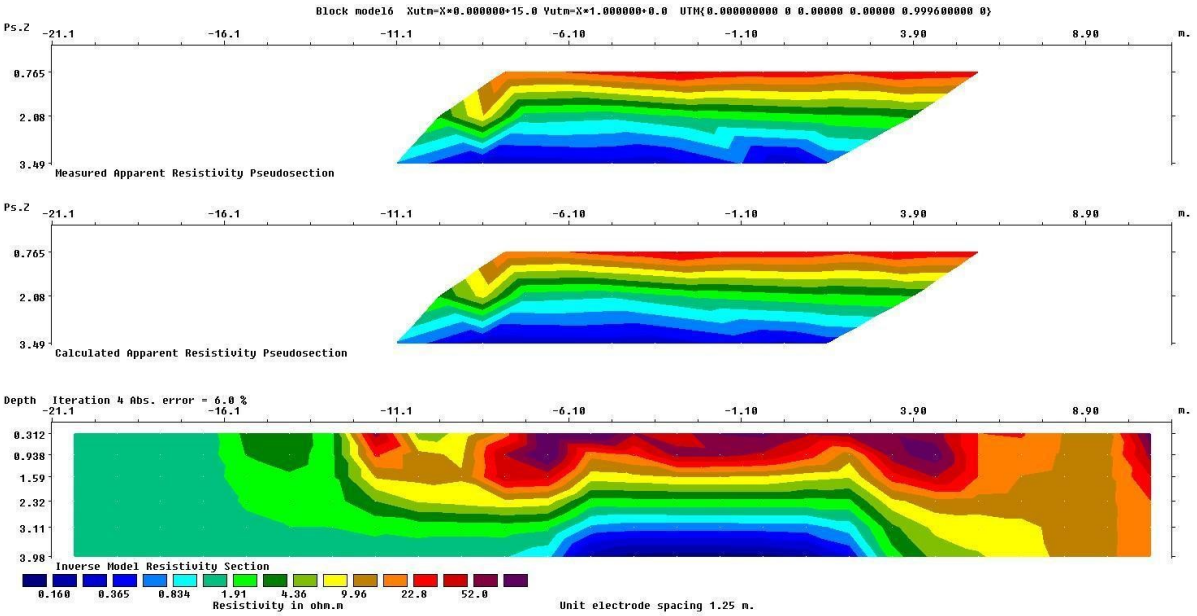

Figure 7.26. 2D inversion model for line number 6

As the main focus of the thesis revolves around conducting a comparative study, our objective is to present a 3D representation of the OhmMapper survey derived from 2D line data. This entails collating the 2D surveys corresponding to each of the six lines into a unified 3D data format. To address this issue, we employed RESIPy software to solve the issue. Initially, we need to select the option for generating a 3D survey from 2D lines. Subsequently, the data exported in RES2DINV format should be simultaneously dragged into the software interface.

Upon importing the data into the software, given that the data have already undergone processing, we proceed directly to the inversion settings. Within this tab, it's important to employ normal regularization and adjust the number of iterations to four. It's recommended to estimate a_wgt and b_wgt based on error checks in the field data, preferably derived from reciprocal measurements rather than repeatability measures. Typically, for surface data, a_wgt is approximately zero ohms, while b_wgt is around 0.01, roughly corresponding to a 1% error. Once all essential inversion parameters are adjusted, the 3D inversion model can be visualized **(Figure**

7.27), and display horizontal section in surface **(Figure 7.28)**, at depth of 1.5m**(Figure 7.29)**, and depth of 2.5m**(Figure 7.30)** and vertical section when Y=0 **(Figure 7.31)**.

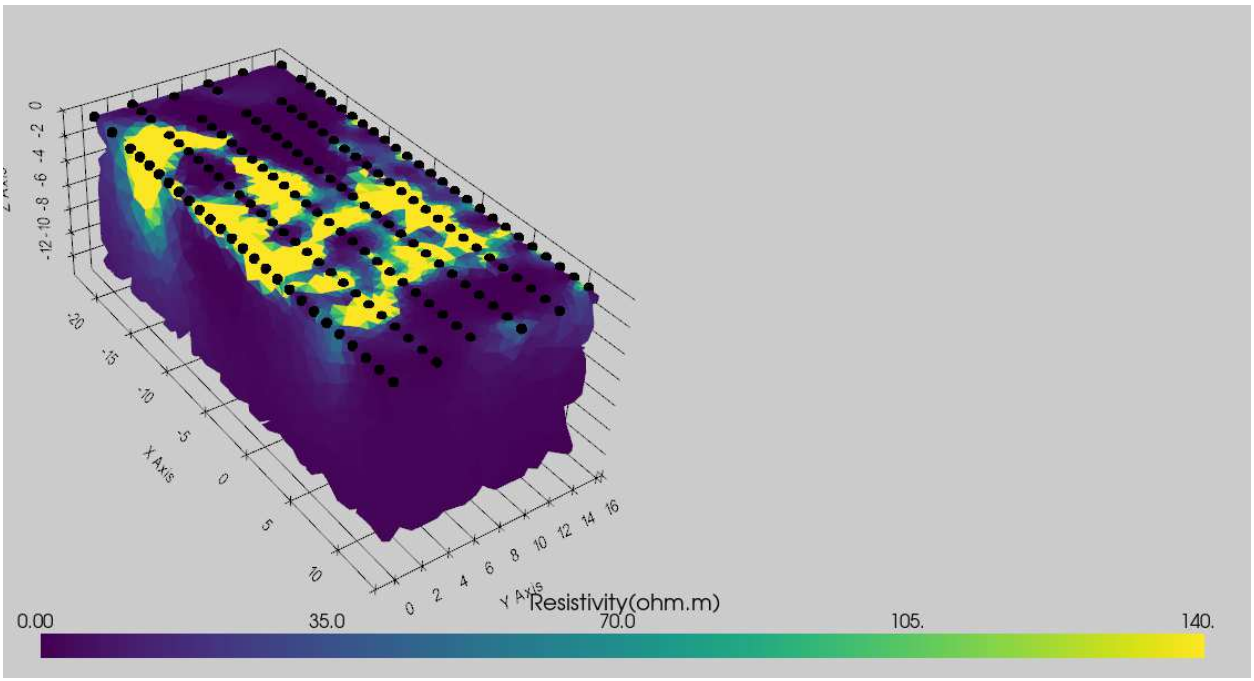

Figure 7.27. Visualize 3D Ohm mapper inversion model

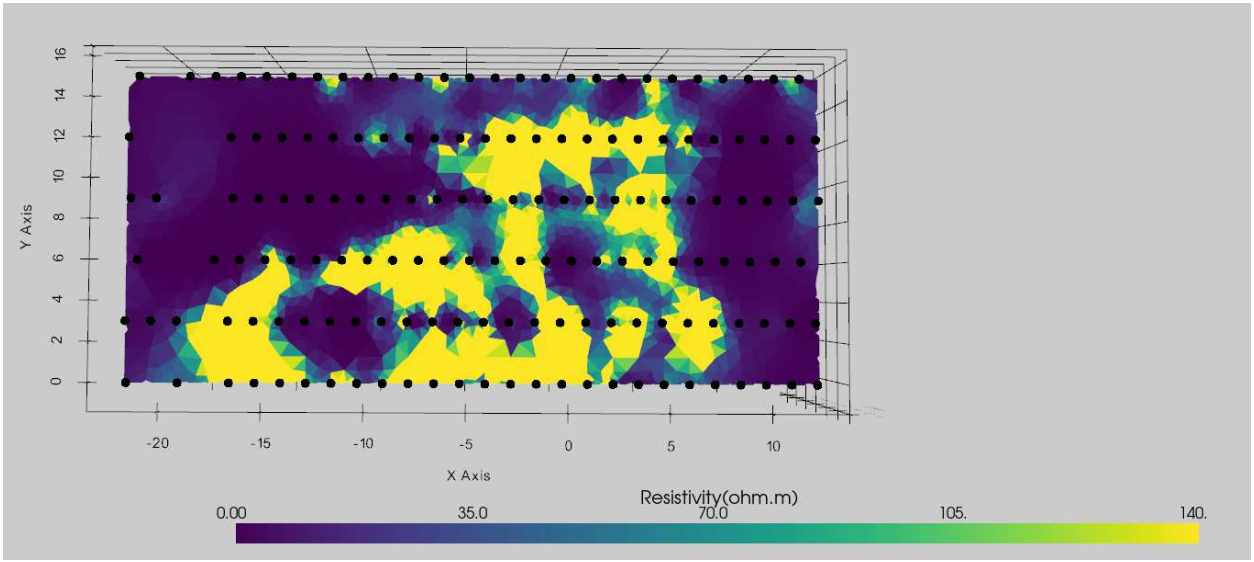

Figure 7.28. 3D inversion model, Horizontal section, slice xy, Z=0

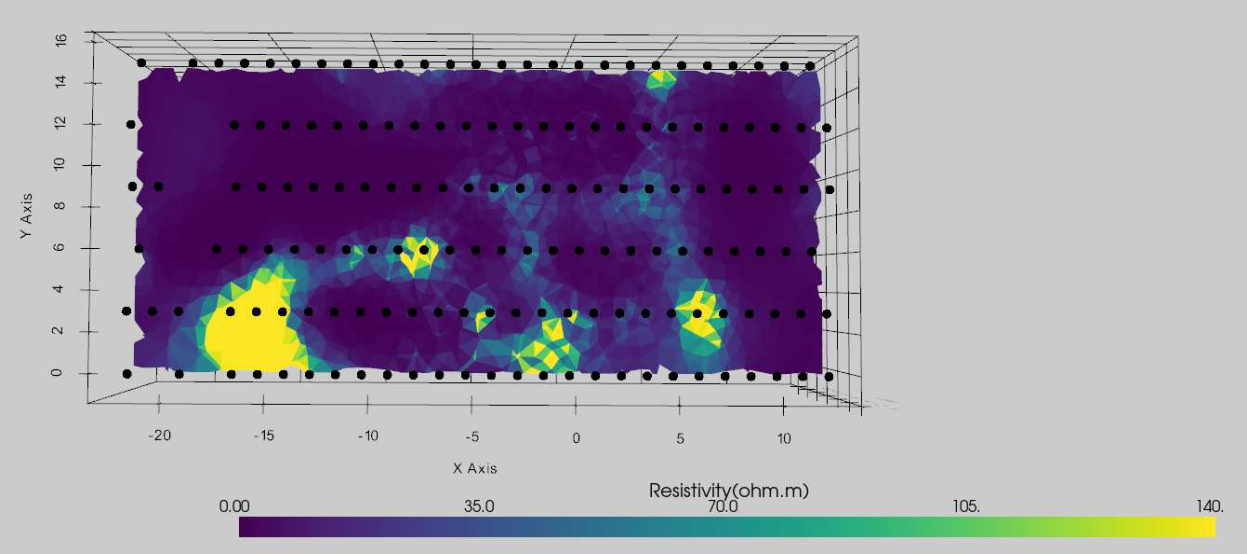

Figure 7.29. 3D inversion model, Horizontal section, slice xy, Z=1.5

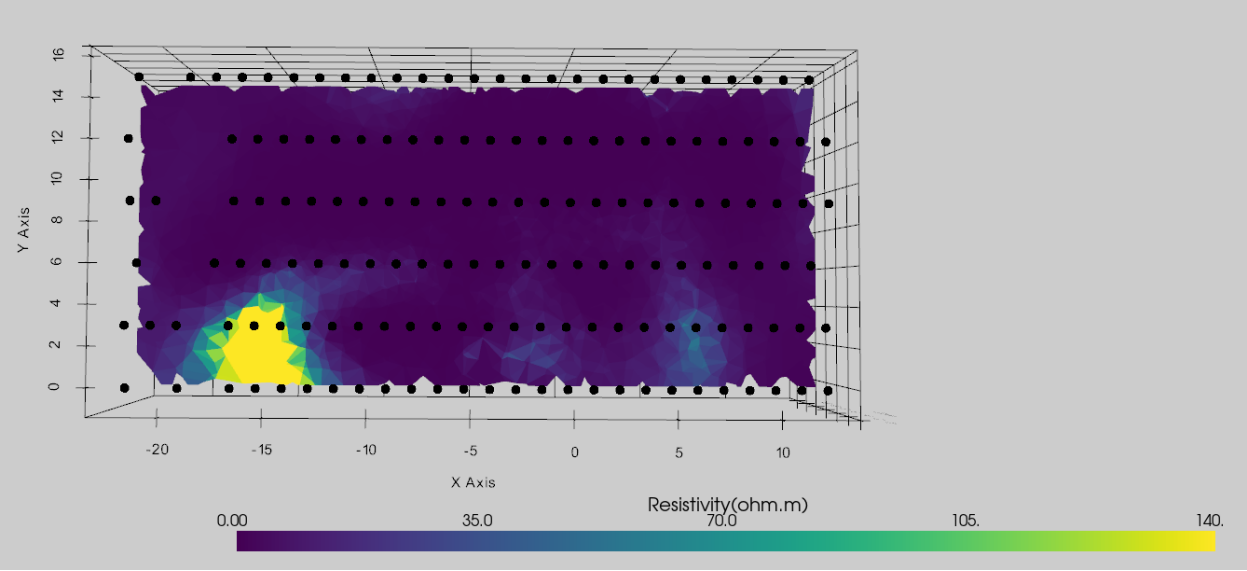

Figure 7.30. 3D inversion model, Horizontal section, slice xy, Z=2.5

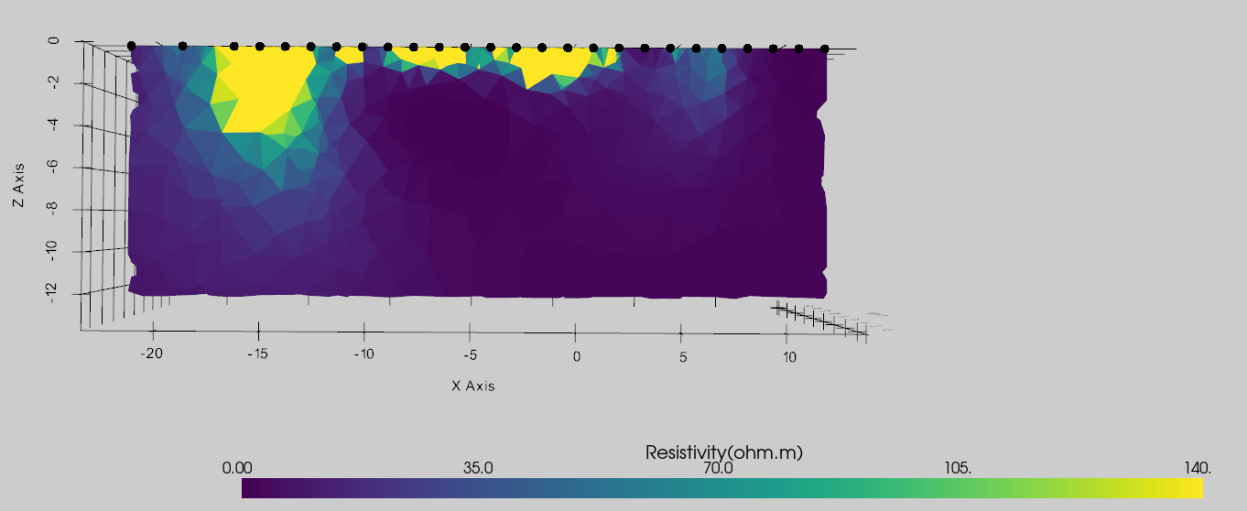

Figure 7.31. 3D inversion model, vertical section, slice xz, Y=0

8. Discussion

Our main hypothesis states that the soil electrical variation constitutes a tool for interpreting soil water content. The electrical resistivity variation can be interpreted as soil moisture variation. Resistivities are specific to each soil type, since they depend on several soil properties such as porosity, cation exchange capacity, organic matter content, salinity or clay content **(Figure 5.2)**. The expected relationship of resistivity and soil moisture is inverse, since reduction of the liquid phase decreases charge mobility (anions and electrons). Muñoz-Castelblanco et al found that variations in the degree of water saturation corresponded to variations in electrical resistivity from resistivity data at 1 m of depth and at 3m of depth [22]. **Figure7.16** and **Figure 7.27** present the 3D ERT and Ohm mapper data inversion model. One vertical section (y=0) and three horizontal sections z=0, z = −1.5m and z =−2.5m were chosen as representative examples for both measurements.

The vertical profile result from 3D ERT inversion **(Figure7.20)** shows low values of resistivity (10–35 Ω) in surface and subsurface at the 1m-2m of depth along all parts of the profile. This resistivity was associated with high water content (40%–80%). So, Soil with clay content is more conductive. Also, Horizontal profile (Z=0) **(Figure7.17)** shows soil pockets of soil with high resistivity value

more than 100Ω, it is important to highlight the discordance of high resistivity (>100) and low moisture values (0–10%) observed for depths of 0-50 cm.

According to the vertical profile resulting from Ohm mapper data inversion model **(Figure 7.31),** it's clear to see more discordance of high resistivity (>100) and low moisture values observed along all parts of the profile (-10m–5m). In this study, the ERT and ohm mapper profiles were carried out very close to the vineyard; these anomalies resulted from the presence of roots. This suggests that water may be retained in soil sub-superficial layers (1.5-2m of depths), likely as a result of root system action, and this suggests an effect in water movement by root water uptake. According to the horizontal profiles at the depths of zero, 1.5 m, and 2.5m derived from the Ohm mapper data inversion model, there is a decrease in these soil pockets with high resistivity values (>100) as the depth increases. This suggests that the maximum depth of the root may lie between 1.5m and 2.5m. However, the ERT inversion results were unable to precisely determine the depth of the root.

The profile result from ERT inversion at the depth from 2m to 5m showed moderate values of resistivity (35Ω–70Ω) along the central part of the profile (4m–12m). This resistivity was associated with low water content (40%–60%). highly resistive soil was located over this area, showing the same parts with high resistivities (up to 140 Ω) which were shown in ohm mapper inversion as a result of reduced water availability (10% moisture) for roots. Profiles around both sides of this range showed lower resistivity values (10Ω–35Ω) with increased moisture values (60%–80%). It is important to highlight the low resistivity value (<35) and high moisture values observed for depth from2m to 5m, because maybe it's a clue to determine the status of the water table.

According to the vertical profile result from ohm mapper inversion **(Figure 7.31),** it's clear to see more low resistivity values (<35) and high moisture values observed along all parts of the profile (-10m–5m) associated with ohm mapper data inversion result at the depth from 2m to 5m. It means that there is an expectation to visit a water table below the root system.

9. Conclusion

The findings from both the 3D ERT inversion and Ohm mapper data inversion models indicate an inverse correlation between soil moisture and resistivity. Given the high sensitivity of the ohm mapper, it was anticipated that the ohm mapper inversion model would yield higher resolution results compared to the 3D ERT inversion model.

In the 3D ERT inversion model, soil pockets were identified at a depth of 50 cm with high resistivity (>100) near where measurements were taken in the vineyard, suggesting potential root presence. The Ohm mapper inversion model revealed additional soil pockets with high resistivity (>100) extending to depths of 2m-2.5m, indicating a maximum root depth between 1.5m and 2.5m.

Moreover, the 3D ERT inversion model depicted soil with moderate resistivity (between 70-35) beyond 2m depth, alongside areas near roots exhibiting high resistivity (>100), suggesting a gradual decrease in water availability near the roots. Additionally, soil with low resistivity (<35) beyond 2m depth implied the potential presence of a water table, a finding corroborated by the Ohm mapper inversion model, which also identified significant amounts of low resistivity soil, indicative of a water table near the roots at depths exceeding 2m-2.5m. All results from ohm mapper inversion indicate that this instrument could be useful for assessing the root system.

Overall, the resistivity distribution observed through the ERT inversion profile appeared more heterogeneous compared to the Ohm mapper inversion profile, particularly beyond a depth of 2m, likely due to the significant influence of roots on ERT results. Ohm mapper could be a useful tool for obtaining the best image with high resolution related to subsurface, and shows maximum depth of root, and water table. ERT method could be a useful tool for estimating soil moisture. The vineyard's location in an area with clay-rich soil could significantly impact resistivity values.

Moisture content primarily influenced resistivity values, with resistivities > 70Ω associated with moisture contents ranging from 10% to 40%, resistivities between 35Ω–70Ω linked to moisture contents of 20% to 60%, and resistivities <35Ω associated with moisture contents of 40% to 80%, depending on depth.

Considering the differences between both methods, using the joint inversion method is a useful method to obtain the best high-resolution image of the condition under the ground, which can provide all the required information, including soil moisture, root condition, root depth, and water table.

References

[1]	K. O'Keefe, "Brunello di Montalcino: Understanding and Appreciating One of Italy's greatesr wines", Berkeley,Los Angles, London: University of California, 2012, pp. 13-16.
[2]	G. Masellis, ""Montalcino et son Brunello : évolution et succès"," Université de Bourgogne, Burgundy, September,2014.
[3]	A. M. M. C. P. D. D. Luiz Fernando de N. Vianna∗, "" Evaluating environmental factors, geographic scale and methods for viticultural zoning in the high-altitude region of Santa Catarina, Brazil"," *Elsevior,* pp. 1-2, 2018.
[4]	H. Ulukan, ""Agronomic Adaptation of Some Field Crops: A General Approach"," *REVIEW ARTICLE,* pp. 2-4, 2008.
[5]	P. D. Cornelis van Leeuwena, ""The Impact of Climate Change on Viticulture and"," *Journal of Wine Economics,* pp. 3-4, 2015.
[6]	1. E. S. A. L. a. L. M. David R. Smart, ""Grapevine Rooting Patterns: A Comprehensive Analysis and a Review"," *From Proceedings of the Soil Environment and Vine Mineral Nutrition Symposium,* pp. 1-5, 2006.
[7]	A. C.-P. Víctor Macías-Carranza, ""Climatology and evapotranspiration in wine valleys of Baja California"," p. 2, 2021.
[8]	E. L. M. V. &. A. Pellegrino1, ""Relationships between plant and soil water status in vine"," *Plant and Soil,* pp. 3-9, 2004.
[9]	2. J. C. D. M. ,. P. P. ,. D. O. a. T. P. V. PHOGAT1, ""Historical and future trends in evapotranspiration components and irrigation requirement of winegrapes"," *Australian Journal of Grape and Wine Research,* pp. 1-2, 2020.
[10]	3. M. C. a. G. S. H. PAUL R. PETRIE1, ""Growth and dry matter partitioning of Pinot Noir (Vitis vinifera L.) in relation to leaf area and crop load"," *Australian Journal of Grape and Wine Research,* p. 1, 2000.
[11]	M. F. A. A. S. Gerardo ECHEVERRÍA, ""SOLAR RADIATION DISTRIBUTION IN THE URUGUAYAN COAST OF THE RIO DE LA PLATA AND ITS RELATIONSHIP WITH VITICULTURAL CLIMATE"," p. 2.
[12]	J. M. Huggett, ""Geology and wine: a review"," *Article in Proceedings of the Geologists Association,* pp. 3-9, 2006.

[13]	A. Maltman, ""The Role of Vineyard Geology in Wine Typicity"," *Journal of Wine Research,* pp. 3-4, 2008.
[14]	S. Campana, ""Remote Sensing, GIS, GPS e tecniche tradizionali Percorsi integrati per lo studio dei paesaggi archeologici: Murlo-Montalcino e bassa Val di Cornia"," UNIVERSITÀ DI SIENA – UNIVERSITÀ DI PADOVA, UNIVERSITÀ DI PISA – UNIVERSITÀ DI VENEZIA, Siena, 2002.
[15]	S. Campana, ""Carta archeologica della provincia di Siena"," UNIVERSITÀ DEGLI STUDI DI SIENA, Siena, 2013.
[16]	R. B. P. B. G. L. L. L. *. S. P. P. S. EDOARDO A.C. COSTANTINI*, ""Land Peculiarities of the Vine Cultivation Areas in the Province of Siena (Italy), with Indications concerning the Viticultural and Oenological Results of Sangiovese Vine. "," Istituto Sperimentale per l'Enologia, Gaiole in Chianti (SI), Firenze, 2006.
[17]	M. Signorini, ""EFFETTI DI TRATTAMENTI CON INDUTTORI DI RESISTENZA SUI CARATTERI PRODUTTIVI E QUALITATIVI DELLA VARIETÀ SANGIOVESE A MONTALCINO"," UNIVERSITÀ DEGLI STUDI DI VERONA, Verona, 2017.
[18]	,. E. A. C. S. P. BUCELLI1, ""IT IS POSSIBLE TO PREDICT SANGIOVESE WINE QUALITY THROUGH A LIMITED NUMBER OF VARIABLES MEASURED ON THE VINES"," pp. 3-6, 2010.
[19]	E. A. Costantini, ""Zonazione viticola ed olivicola della provincia di Siena"," CRA-Istituto Sperimentale per lo Studio e la Difesa del Suolo di Firenze; Dipartimento di Scienze della Terra, Università di Siena, Siena, 2006.
[20]	E. m. s. Saccone, ""Climate Change Impacts and Adaptations for Small Wine Producers in Central Italy"," Utrecht University, Utrecht, 2021.
[21]	D. M.H.Loke, ""Tutorial : 2-D and 3-D electrical imaging surveys"," 2004.
[22]	J. M. P. P. D. a. Y. J. C. J. A. Muñoz-Castelblanco, ""The influence of changes in water content on the electrical resistivity of a natural unsaturated loess"," *Geotechnical Testing Journal,* p. 12, 2012.